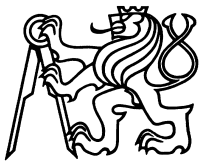

Czech Technical University in Prague
Faculty of Nuclear Sciences and Physical Engineering

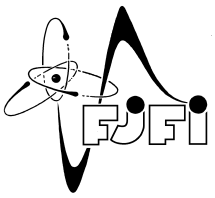

The Cherenkov detector role in the Runaway Electron diagnostics on tokamak COMPASS

Role Čerenkovova detektoru při měření ubíhajících elektronů na tokamaku COMPASS

Research task

Author: **Jaroslav Čeřovský**

Supervisor: **doc., RNDr. Jan Mlynář, Ph.D.**

Academic year: 2016/2017

- Zadání práce -

Acknowledgment:
I would like to thank doc. RNDr. Jan Mlynář, Ph.D. for his expert guidance and express my gratitude to Ing. Ondřej Ficker and RNDr. Eva Macúšová, Ph.D. for their help and valuable advices.

Author's declaration:
I declare that this Research task is entirely my own work and I have listed all the used sources in the bibliography.

Prague, July 7, 2017 Jaroslav Čeřovský

Název práce:

Role Čerenkovova detektoru při měření ubíhajících elektronů na tokamaku COMPASS

Autor: Jaroslav Čeřovský

Obor: Fyzika a technika termojaderné fúze

Druh práce: Výzkumný úkol

Vedoucí práce: RNDr. Jan Mlynář, Ph.D., Ústav fyziky plazmatu AV ČR

Abstrakt: Vysokoenergetické elektrony, tzv. ubíhající elektrony, jsou generovány v tokamacích za určitých podmínek. Tyto elektrony jsou urychlovány elektrickým polem tokamaku téměř beze srážek s termálními částicemi plazmatu až k rychlosti světla a jsou vážnou hrozbou pro budoucí fúzní reaktory. Detektory založené na Čerenkovově jevu byly vyvíjeny a instalovány v posledních letech. Takový detektor může poskytnou měření s vysokým časovým a dobře prostorově definovaným rozlišením. Vyjímečná vlastnost Čerenkovova detektrou spočívá v možnosti přímého pozorování ubíhajících elektronů a tedy se nejedená o nepřímou metodu, která by byla založena na měření tvrdého rentgenového záření nebo neutonů. Studiu ubíhajích elektronů se intezivně věnují na tokamaku COMPASS. Tato práce je zejména věnována analýze dat z Čerenkovova detektoru a charakterizaci ubíhajících elektronů v různých podmínkách. V práci jsou studovány svazky ubíhajících elektronů vzniklých po disrupci a radiální profil Čerenkovova záření, které způsobeno interakcí ubíhajících elektronů s detektorem.

Klíčová slova: Čerenkovův detektor, diagnostika plazmatu ubíhající elektrony, tokamak

Title:

The Cherenkov detector role in the Runaway Electron diagnostics on tokamak COMPASS

Author: Jaroslav Čeřovský

Abstract: High energy electrons - so called runaway electrons - are generated in tokamaks under particular conditions. These electrons are accelerated in the electric field of tokamak almost without collisions with thermal particles nearly to the speed of light and present a serious threat to the future fusion reactors. Detectors based on the Cherenkov radiation have been developed and implemented for the last couple of years. Such a detector may provide high temporal resolution and well defined position of measurements. A unique feature of Cherenkov type detector lies in the possibility of direct observation of runaway electron and therefore it is not an indirect method based on measurements of secondary X-rays and neutrons. Runaway electron (RE) studies are intensively carried out at the COMPASS tokamak. Main focus of this work is the analysis of data from Cherenkov detector and characterization of runaway electrons under different conditions. Post-disruption runaway electron beam and radial dependence of Cherenkov radiation induced by RE in detector are investigated.

Key words: Cherenkov detector, plasma diagnostics, tokamak, runaway electrons

Contents

Introduction

The most promising way how to achieve the limitless and environmentally friendly source of energy is currently thermonuclear fusion. This way of producing energy would ensure an ever-increasing demand for it for the future generations and prevent political struggle for unprocessed materials.

Current research of fusion plasma is focused mainly on tokamaks. Tokamak is a device, which use the strong magnetic field to confine plasma in shape of the torus and current flowing in the torodial direction to heat a plasma and complete the desired helical magnetic configuration. The word tokamak is an abbreviation of the Russian word for the toroidal chamber with magnetic coils. Tokamaks are devices with long history and best experimental results among all concepts of magnetic confinement fusion.

These days the whole fusion community is impatiently waiting for the finishing International Thermonuclear Reactor, called ITER. ITER will prove, whether our ability to control fusion plasma is sufficient and wheter we can think about using thermonuclear reactor as a source of electricity in the future. Even though ITER will show up that electricity production through fusion is possible, there is another threat, which is danger to the ITER itself and mitigation of this threat is crucial for secure operation of future thermonuclear power plants. This threat are runaway electrons.

Runaway electrons are high energy particles, which could cause severe damage by impact to the first wall of the tokamak. Runaway electrons are intensively studied last couple of years for the effort to understand their generation and suppression. Very strong post-disruptive runaway currents are expected in ITER. Understanding of generation and mitigation of runaway electrons can give a chance to ITER to achieve its mission. The phenomenon of runaway electrons in not only a matter of tokamak physics. The lightning strikes are for example explained by the presence of runaway electrons.

New insight into runaway electron issue can be provided by detectors, which are based on the Cherenkov effect. Cherenkov radiation is electromagnetic radiation emitted, when a charged particle passes through a dielectric medium at a speed greater than the phase velocity of light in that medium. Cherenkov-type detector can provide high temporal resolution and well spatially defined measurements. One of the advantages of this type of detector is the possibility of observing in-flight runaway electrons, which are escaping from the plasma. Therefore, it is not an indirect method, which relies on measurements of secondary X-rays or neutrons.

The first chapter of this research task is dedicated to brief introduction into runaway electron physics and calculation of maximal attainable energy of runaway electrons in tokamak COMPASS. Introduction into theory behind the Cherenkov effect is given in the second chapter. The third chapter deals with description of the Cherenkov detector and with summary of results conducted on several tokamaks using the Cherenkov detector. The last fourth chapter is focused mainly on analysis of experimental data from the COMPASS tokamak. The main aim of this work is evaluation of experiments dedicated to runaway electrons via Cherenkov detector on the tokamak COMPASS.

Chapter 1

Runaway electron physics

In the tokamaks the plasma current is generated by the inductively driven electric field in toroidal direction. Same electrical field, which drives current through plasma column, gives rise to runaway electrons. In the simplest case, electrons in the plasma are accelerated by the electrical toroidal field and suffer from the Coulomb collisions with plasma bulk particles. The collisions with other particles in the plasma are slowing down electrons and thus represent friction force, which is trying to balance continuous acceleration. At the moment when accelerating force exceeds the friction force, electrons can run away. In tokamaks runaway electrons can be created during low density discharges due to smaller number of collisions, and during disruptions due to the high induced electric field. This chapter will deal with basics of runaway electrons physics.

1.1 Generation

1.1.1 Primary - Dreicer generation

As mentioned in the introduction to this chapter runaway electrons occur, when electric force $\boldsymbol{F_e} = -e\boldsymbol{E}$ exceeds friction force $\boldsymbol{F_d}(v) = -m_e\nu\boldsymbol{v}$, where ν denotes electron collision frequency. Electron collision frequency for electrons with suprathermal velocities can be expressed by formula [1]

$$\nu = \frac{n_e e^4 \ln(\Lambda)}{4\pi\epsilon^2 m_e^2 v^3}, \tag{1.1}$$

where $\ln(\Lambda)$ denotes Coulomb logarithm. n_e, m_e, ϵ are electron density, electrons mass and vacuum permittivity respectively and v the velocity of the electron. As can be seen from the previous formula friction force is monotonic function of velocity and for high velocities goes to zero. Movement of electron in electrical field can be described by the equation

$$m_e\frac{\mathrm{d}v}{\mathrm{d}t} = eE - m_e\nu v \approx eE - \frac{n_e m_e e^3 \ln(\Lambda)}{4\pi\epsilon^2 m_e^2 v^2}. \tag{1.2}$$

From this equation it is obvious, when right hand side of the equation is negative, electron will be slowed down, but when right side of equation is positive, electron will be accelerated. Whether an electron will be accelerated or decelerated is determined by the value of the initial velocity. Velocity needed to make electron run away, called critical velocity v_c, can be determined from previous equation as

$$v_c = \sqrt{\frac{n_e e^3 \ln\Lambda}{4\pi\epsilon^2 m_e E}}. \tag{1.3}$$

If we assume both electron-electron and electron-ions collisions, expression for critical velocity v_c would have following form [2]

$$v_c = \sqrt{\frac{n_e e^3 \ln\Lambda(2 + Z_{eff})}{4\pi\epsilon^2 m_e E}}. \tag{1.4}$$

Here Z_{eff} is the effective charge number of the ions, which is define as $Z_{eff} = \frac{\sum_i n_i Z_i}{n_e}$. Runaway electrons have therefore a kinetic energy of at least W_c:

$$W_c = \frac{1}{2} m_e u_c^2 \approx 2,2(2 + Z_{eff}) \frac{n_e[10^{-19}\mathrm{m}^{-3}]}{E[\mathrm{V/m}]}\mathrm{keV}. \tag{1.5}$$

For example, if we assume $Z_{eff} = 1,5$, $n_e = 2 \cdot 10^{-19}$ m^{-3} and $E = 0.2$ V/m, critical energy is approximately 58 keV. Actually, collisional frequency is not decreasing function of velocity in whole range of velocities [3]. For velocities smaller than thermal velocity v_T collisional frequency is independent on velocity and thus drag force is increasing linearly with increasing velocity of the particle. The faster a particle move, the more particles experience collisions. The maximum of the drag force is around the electron thermal velocity v_T and then decreasing as $\propto \frac{1}{v^2}$.

If we take a look at Fig. 1.1, intersections of curves, which belong to force of the electrical field (green one) and drag force caused by collisions with plasma particle (blue one), divide figure into three velocity regions. In region I. force of electrical field is dominating and electrons will be accelerated up to velocity at which both forces are equal. In region II. friction force is greater than accelerating force and thus electrons will be slowed down. In region III. force of electrical field dominates again, but there isn't any stable point and electrons will run away.

The type of runaway electron generation described in this section is in the literature called Dreicer generation [4, 5] and is associated with Dreicer field E_D. This field approximately balances maximum of the friction force. The Dreicer field is given by

$$E_D = \frac{n_e e^3 \ln\Lambda}{4\pi\epsilon^2 k T_e}, \tag{1.6}$$

where T_e is temperature of electrons and k is the Boltzmann constant. An approximate expression for growth rate of the runaway electron population [6, 7, 8] due to this type of generation is

$$\frac{\mathrm{d}n_r}{\mathrm{d}t} = C n_e \nu_{th} \varepsilon^{-3(1+Z_{eff}/16)} \exp\left(-\frac{1}{4\epsilon} - \sqrt{\frac{1 + Z_{eff}}{\varepsilon}} \right). \tag{1.7}$$

Here n_r is the runaway electron density, $\epsilon = \frac{E}{E_D}$, C in constant of order unity not determined by the analytic model and ν_{th} is electron-electron collision frequency of thermal particles, which is given by

$$\nu_{th} = \frac{n_e e^4 \ln\Lambda}{4\pi\epsilon^2 m_e^2 v_{th}^3}. \tag{1.8}$$

The Dreicer field E_D corresponds to the field balancing the maximum of the friction force. The critical field E_c, on the other hand, is roughly equivalent to the minimum of the collisional friction force. The critical field [8] is the weakest field at which is runaway possible and its value is given by

$$E_c = \frac{n_e e^3 \ln\Lambda}{4\pi\epsilon^2 m_e c^2}, \tag{1.9}$$

where c is speed of light. When $E > E_c$, there exist some critical velocity v_c above which the electric field overcomes the friction force. Particles with a velocity greater than critical velocity will run away.

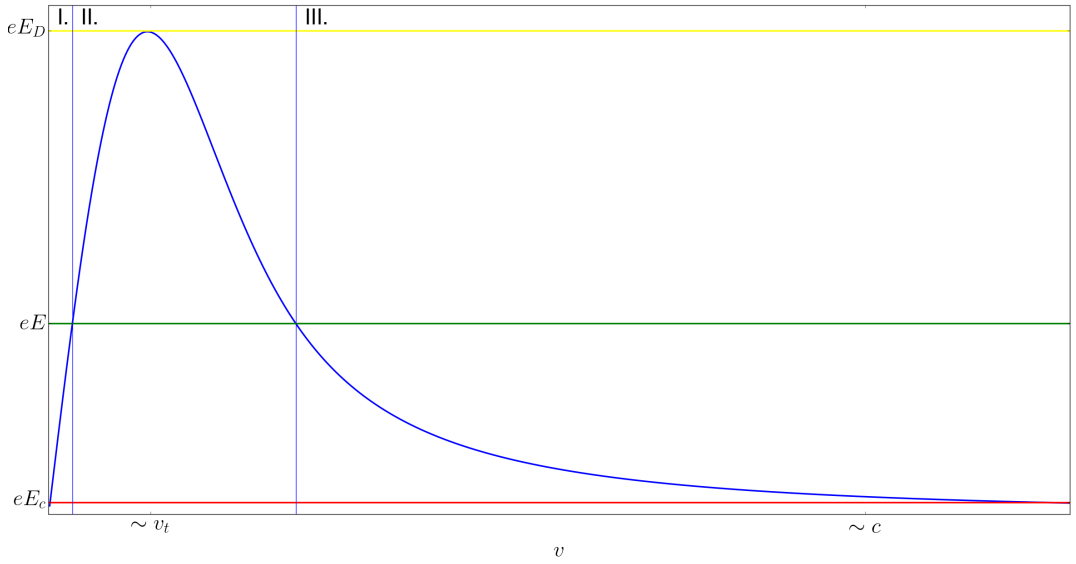

Figure 1.1: A graph of friction force as an demonstration of the Dreicer mechanism. The friction force is represented by the blue curve and the accelerating force of electric field corresponds to the green line. Intersections of these two curves divide the figure into three regions. The border of the region I. and II. is stable, because when electron gain enough velocity and enters the region II., the friction force will increase and electron will be slowed down. On the other hand, when electron lose his velocity and enters to the region I., force of the electric field, which is here dominating, will speed it up. The border between region II. and III. is unstable. All particles to the right from this border are accelerated to the high velocities and run away.

On the contrary, particle with sub-critical velocity will be slowed down to the thermal speed. When $E < E_c$, there is no way for particles to run away.

1.1.2 Hot tail generation

Hot tail runaway generation process [9] significantly differs from Dreicer mechanism, which was described in previous section, and is associated with plasma instability. Hot tail runaway electron generation is caused by incomplete thermalization of the electron velocity distribution during rapid plasma cooling. It is the most important runaway electron mechanism in tokamak disruption if the thermal quench is fast enough.

During rapid cooling of plasma, which can be caused for example by massive gas injection (MGI), electrons are decelerated by ionization and deexcitation of plasma impurities. Electrons with high velocities (from the tail of Maxwellian distribution) have low collisional frequency and almost do not collide during the thermal quench, because their average collision time τ (reversed value of collision frequency ν) is comparable or longer than thermal quench time t_0.

1.1.3 Secondary generation

One of the most interesting and important types of runaway generation is secondary generation, called avalanche mechanism [10]. Secondary runaways are formed when existing runaways collide with thermal electrons and runaways transfer enough momentum to the thermal electron to kick it into the runaway region while incoming electron remains runaway itself. This type of collision is referred to as knock-on collision and is rare in tokamak plasma. From this simple idea it follows that the smallest energy of incoming particle must fullfill inequality $W_i > 2W_c$, where W_i is energy of incoming particle and W_c is critical energy. In other words, the kinetic energy of incoming particle must be at least twice as large as the critical energy.

Secondary mechanism of generation runaway electrons is the most important way of production for large tokamak and it will be crucial for ITER. For ITER avalanche mechanism will be much more important than direct Dreicer mechanism. The avalanche growth rate takes the form [10]

$$\frac{\mathrm{d}n_r}{\mathrm{d}t} = \frac{n_r(E_r - 1)}{\tau \ln \Lambda} \sqrt{\frac{\pi\Gamma}{3(Z_{eff} + 5)}}(1 - E_r + \frac{4\pi(Z_eff + 1)^2}{3\Gamma(Z_eff + 5)(E_r^2 + 4/\Gamma^2 - 1)})^{-1/2}, \tag{1.10}$$

where $E_r = \frac{|E_\parallel|}{E_c}$ is the relative strength of the electric field, Γ is so called neoclassical function and describes the effects of the toroidal geometry and $\tau = \frac{m_0 c}{cE_c}$. Neoclassical function Γ is function of inverse aspect ratio and can be roughly expressed as

$$\Gamma \approx (1 + 1,46\sqrt{\varepsilon} + 1,72\varepsilon)^{-1}. \tag{1.11}$$

The equation (1.10) takes a more simple form for very strong field ($E_r \gg 1$), $Z_eff = 1$ and large aspect ratio ($\varepsilon \to 0$)

$$\frac{\mathrm{d}n_r}{\mathrm{d}t} = \sqrt{\frac{\pi}{2}} \frac{n_r}{3\tau \ln \Lambda}(E_r - 1) \tag{1.12}$$

This production rate is proportional to n_r and leads to an exponential growth of n_r. Dreicer mechanism or other generation mechanism of runaway electrons can lead to the runaway electron growth and provide a seed for the secondary generation. Later time the secondary generation process dominates. In a disruption, the Dreicer and the hot tail processes are primary runaway mechanisms, which create a runaway electron seed population. This population is amplified by secondary avalanche mechanism [11].

1.1.4 Other mechanisms of generation

In addition to the mechanism described above, there are several other ways leading to creation of the runaway electron seed. In ITER, tritium and Compton scattering of γ-rays emitted by the wall are possible RE sources. The magnitude of the RE generation rate from γ-rays Compton scattering depends on the activation of the wall and is uncertain, but cannot be neglected, when Dreicer generation is suppressed and hot tail generation is absent.

1.2 Energy limit of runaway electrons

When an electron exceeds the critical velocity (1.3) it is permanently accelerated by the electrical field and can reach high energies, but the energy can be limited by several effects:

- **Orbit displacement limit.** In tokamaks, orbits of runaway electrons are shifted from the magnetic surfaces as a result of curvature and gradient $\boldsymbol{B}$ drift. Considering this displacement we can determine some restriction on maximum attainable energy of runaway electron. The orbit shift δ [2] from the magnetic surfaces can be roughly expressed by

$$\delta \approx \frac{\bar{q}W}{ecB_\phi}, \tag{1.13}$$

  where $\bar{q} = \langle r/B_\theta \rangle B_\phi/R$ is average safety factor, W is the energy of runway electron, e is elementary charge and B_ϕ is magnitude of toroidal magnetic field. Therefore maximum energy due to the orbit displacement is $W_{max}^{shift} \approx aecB_\phi/q_a$. If we assume typical Compass parameters $a = 0,23$ m, $B_\phi = 1,15$ T, $q_a = 3$, we get $W_{max}^{shift} = 26$ MeV. With a more precise treatment of the runaway drift orbits and displacements for different current profiles, which was done in [12] , we will get the following formula for maximum energy of runaway electron

$$W_{max}^{shift} = \frac{R_0 I_p c}{a I_A v_\parallel} \frac{B_\theta(r^*)}{(1 + s'(a))B_\theta(a)}. \tag{1.14}$$

  Here $I_A = \frac{4\pi m_e c}{\mu_0 e}$ is the Alfvén current. The most distant point of the runaway electron orbit is $r^* = r - s(r)$, where $s(r)$ is the Shafranov shift. The shift between the geometrical center and the center of the magnetic flux surface. $s'(a)$ is the first derivative of this shift on the plasma boundary.

  In expression (1.13), we assume that runaway electrons are generated in geometrical center of tokamak. Is is possible to derive formula , which covers this issue [13]. Than we can express maximum accessible electron energy as

$$W_{max}^{orbit} = m_0 c^2 \left(\sqrt{1 + \left[\left(1 - \frac{\rho}{a} \right) \frac{2R_0 I_p}{a * I_A} \right]} - 1 \right), \tag{1.15}$$

  where m_0 is rest energy of electron, c is speed of light, a is minor radius, R_0 denotes major radius, I_p is plasma current and I_A is the Alfvén current.

- **Synchrotron radiation limit.** Synchrotron radiation is the radiation which occurs when charged particles are accelerated in curve path or orbit. The total radiated power P_{syn} of synchrotron radiation emitted by the single electron is described by formula [14]

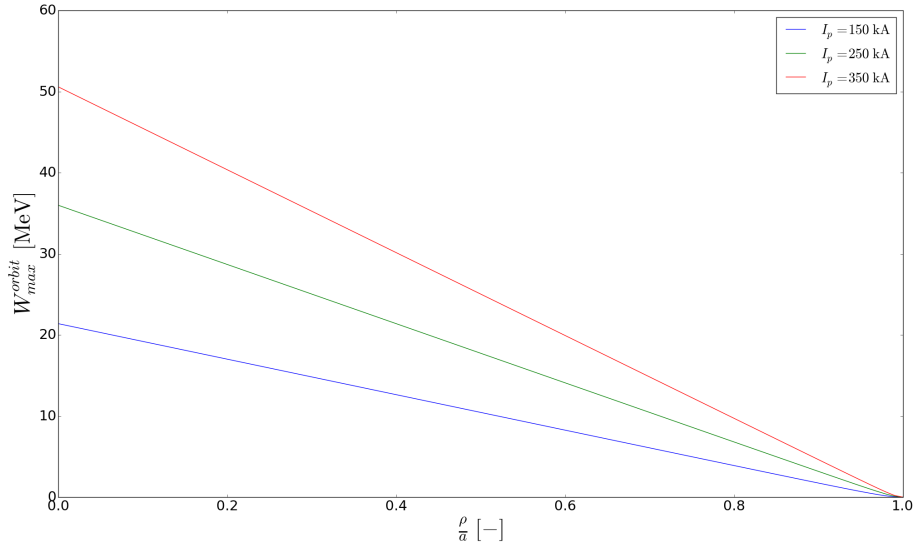

Figure 1.2: Maximal energy for runaway electrons generated at different plasma radii in the Compass tokamak at three different plasma currents calculated using expression (1.15).

$$P_{syn} = \frac{e^2 c}{6\pi\epsilon_0}\frac{\beta^4\gamma^4}{R_c} = \frac{2}{3}\frac{r_e m_e c^3}{R_c^2}\beta^4\gamma^4, \tag{1.16}$$

where $\beta = \frac{v}{c}$, $\gamma = \frac{1}{\sqrt{1-\beta^2}}$ is Lorentz factor, r_e is classical electron radius and R_c is the radius of curvature of the track in the magnetic field. The R_c [15] can be for helical orbit approximated by

$$\frac{1}{R_c} \approx \frac{1-\Theta^2}{R_0} + \frac{eB\Theta}{m_e c\gamma} \tag{1.17}$$

Here $\Theta = \frac{v_\perp}{v_\parallel}$ denotes pitch angle of runaway electron. In tokamaks particles gain energy from the electric field. Power absorbed from the electric field can be expressed as $P_{gain} = ec\frac{U_l}{2\pi R_0}$, where U_l is loop voltage and R_0 is major radius of the tokamak. If we calculate power balance between power loss by synchrotron radiation and power gain from the electric field, we can estimate maximum attainable energy $W_{max}^{syn} = m_0 c^2(\gamma_{max} - 1)$, where γ_{max} is given by

$$\gamma_{max} = -\frac{eR_0 B}{2m_e c}\left(\frac{\Theta}{1-\Theta^2}\right) + \frac{R_0}{2(1-\Theta^2)}\sqrt{\left(\frac{eB\Theta^2}{m_e c}\right)^2 + 4(1-\Theta^2)\sqrt{\frac{3\epsilon_0 U_l}{eR_0^3}}}. \tag{1.18}$$

In the Fig. 1.3, the dependence of maximum attainable energy of runaway electron due to synchrotron radiation limit W_{max}^{syn} on pitch angle Θ is shown for three different value of magnetic field B.

- **Magnetic field ripple limit.** Magnetic ripples are small variations in the magnetic field of tokamak, which are caused by the finite number of the toroidal field coils. Considering N toroidal field coils, the toroidal field is modulated and its modulation frequency is $\omega_r = \frac{nNc}{R_0}$, where n is the harmonic number. It was shown [16] , that if the electron cyclotron motion is in resonance with

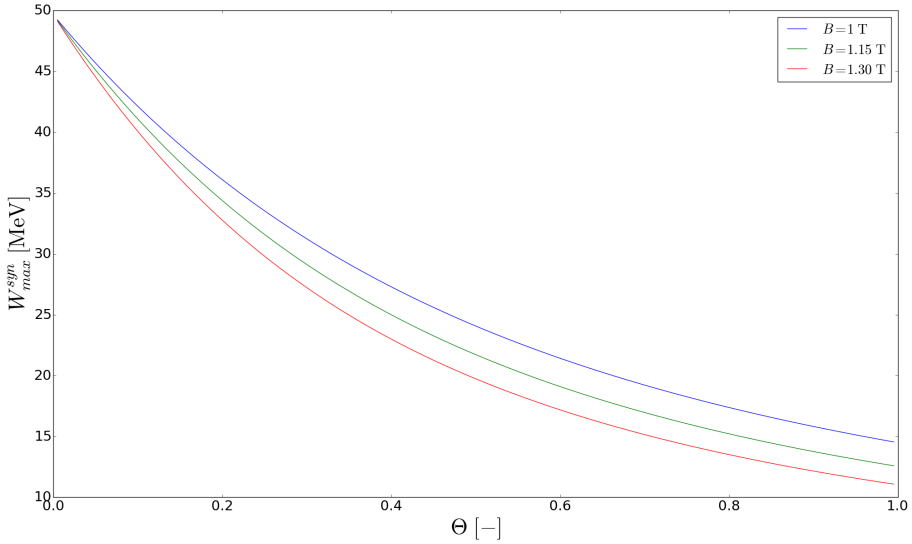

Figure 1.3: The figure shows dependence of maximum achievable energy W_{max}^{syn} of runaway electron caused by synchotron emission on runaway electron pitch angle Θ. This dependence is shown for three different magnitudes of the toroidal magnetic field B. The loop voltage U_{loop} was set to 1 V.

the modulation frequency of the magnetic field, electrons are scattered in pitch angle Θ. This effect can increase pitch angle Θ and thus decrease synchrotron radiation limit. Cyclotron frequency of the relativistic electron may be expressed as $\omega_c = \frac{eB}{m_e\gamma}$. Electron will be in resonance, when $\omega_c = \omega_r$. From this equation follows

$$\gamma = \frac{eBR_0}{nNcm_e}, \qquad W_{max}^{ripple} = 299.8\frac{BR_0}{nN}\ \text{MeV}. \tag{1.19}$$

For Compass tokamak, where $R_0 = 0,56$ m, $B = 1,15$ T, $N = 16$ and the second harmonic frequency ($n = 2$), one gets $W_{max}^{ripple} = 6$ MeV.

- **Time limit.** The most trivial limit to the attainable runaway electron energy is total available time for acceleration to the high energies. If the radiation losses are neglected, the maximum energy to reached by a runaway electron in a single loop may be estimated from a simple formula

$$W_{max}^{time} \approx ec\int \frac{V_l}{2\pi R_0}\,dt = \frac{ec}{2\pi R_0}\Phi(t), \tag{1.20}$$

where $\Phi(t)$ is the flux swing applied to the plasma. For Compass tokamak, the formula (1.20) has a form $W_{max}^{time} \approx 85\Phi(t)$ MeV.

- **Instabilities.** A lot of instabilities can cause looses of runaway electrons and thus prevent them from constantly increasing their energy. Population of runaway electrons can be influenced by presence of magnetic islands [17], by a saw-tooth instability [18] or by resonant magnetic perturbations, which can be applied to the plasma. Another group of instabilities are the kinetic instabilities. These instabilities are mostly caused by non-isotropic distribution function of electrons. One of these is called Parail-Potgutse instability [19] after the scientists that provided theoretical

description. The beam of runaway electrons can generate waves via anomalous Doppler effect and then this waves can be responsible for scattering of high energy electrons in velocity space. When the perpendicular component of velocity is increased, it can result in prompt loss of runaway electrons. Following conditions must be met to develop this instability:

$$\omega_{ce} > \omega_{pe} \qquad v_b > 3\left(\frac{\omega_{ce}}{\omega_{pe}}\right)^{\frac{3}{2}} v_c, \tag{1.21}$$

where $\omega_{ce} = \frac{eB}{m_e}$ is cyclotron frequency of electron, $\omega_{pe} = \sqrt{\frac{e^2 n_e}{\epsilon_0 m}}$ is plasma frequency (n_e denotes density of electrons), v_b is velocity of runaway electrons and v_c is critical velocity given by expression (1.3).

Chapter 2

Cherenkov radiation

When a charged particle travels through a dielectric medium, it polarizes atoms of dielectric medium around it and causes them to briefly radiate as they relax to original state. When a particle is moving slowly the polarization is symmetrical and no significant radiative output is observed. If a particle is moving faster than the phase velocity of the light in the dielectric medium, then its own electromagnetic field is travelling slower than particle and it results in an asymmetry in polarization. Asymmetrical polarization causes the radiation, which is emitted in the direction of the motion. The physical principle of origin of the radiation mentioned above, is demonstrated in the Fig. 2.1.This radiation is called Cherenkov radiation [20, 21], named after Soviet scientist Pavel Alekseyevich Cherenkov.

2.1 Derivation of propertirs of Cherenkov radiation

In this section we will show simple derivation of properties of Cherenkov radiation. We will use only classical approach, which is based only on Huygens principle of geometric relationships between propagating wave and moving particle. During derivation we will use Fig. 2.1.

Now we will show that the condition for emitting the Cherenkov radiation is that the speed of charged particle in dielectric medium must be greater or equal to the phase velocity of light in the medium. We define, that the particle travels with the velocity v_p. The emitted electromagnetic waves propagate with the velocity given by $v_w = \frac{c}{n}$, where n denotes refractive index of the medium. If we take a look on Fig. 2.1, left picture corresponds to the situation on Fig. 2.1 for the non-relativistic case. But the right picture in the Fig. 2.1 represents the relativistic case in the Fig. 2.1.

In the right picture in the Fig. 2.1 equiphase surfaces and shock front are shown, which is result of constructive interference of arising waves. In the picture right-angled triangle with two known side size is marked. Left corner of the triangle represents the location of the particle in time $t = 0$ and right corner of the triangle corresponds to the position of particle in some time t. In a given time t, the particle travels the distance $d_p = v_p t$, but the emitted electromagnetic waves travel only the distance given by $d_w = v_w t$. If we use, that relationships between sides in the right-angled triangle, on can get

$$\cos\theta_c = \frac{1}{\beta n}, \tag{2.1}$$

where θ_c is the Cherenkov angle. The electromagnetic radiation is emitted in the cone with angle Θ around the direction of propagation of particle. From the equation (2.1) follows that the particle velocity must fulfill condition $n\beta > 1$. With this condition one can compute the minimum energy of particle to have in order to emit Cherenkov radiation as

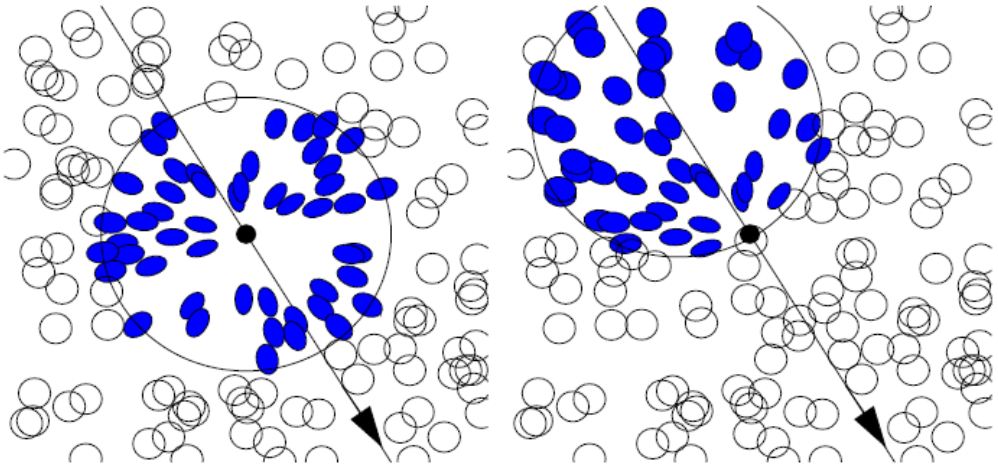

(a) Non-Relativistic (b) Relativistic

Figure 2.1: In this figure it is shown particle travelling through the dielectric medium. The atoms of the medium are indicated by the circles. The area significantly influenced by the charged particle is marked by huge circle and the atoms within are painted blue. The atoms in this area are polarised and oriented towards the moving charged particle. In the non-relativistic case, the atoms in the polarised area are situated symmetrically (the region of influence is centred on the charged particle) and this configuration results in destructive interference of any radiation induced by moving particle. In relativistic case, the region of influence is not centered on the charged particle any more and is located behind the charged particle. This feature result in orientation of particles in a single direction and thus allows constructive interference of emitted radiation. This figure was taken from publication [22].

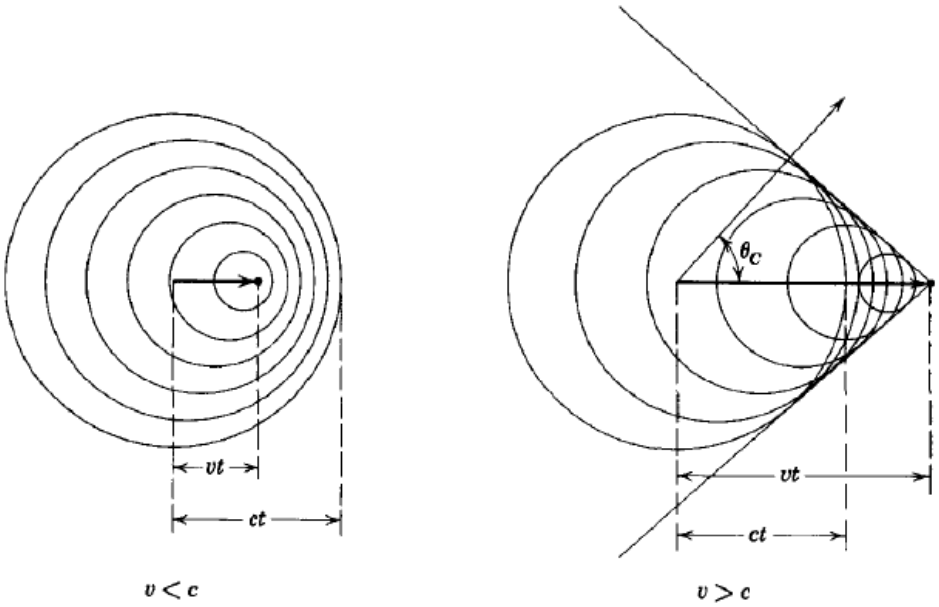

Figure 2.2: A picture illustrating the origin of Cherenkov radiation. The left plot shows particle travelling slowly in dielectric medium and the electromagnetic waves excited by it. The right plot shows particle moving a larger velocity than the phase velocity of light in dielectric medium. An electromagnetic shock wave appears, moving in the direction given by the Cherenkov angle θ_c. This figure was taken from publication [23].

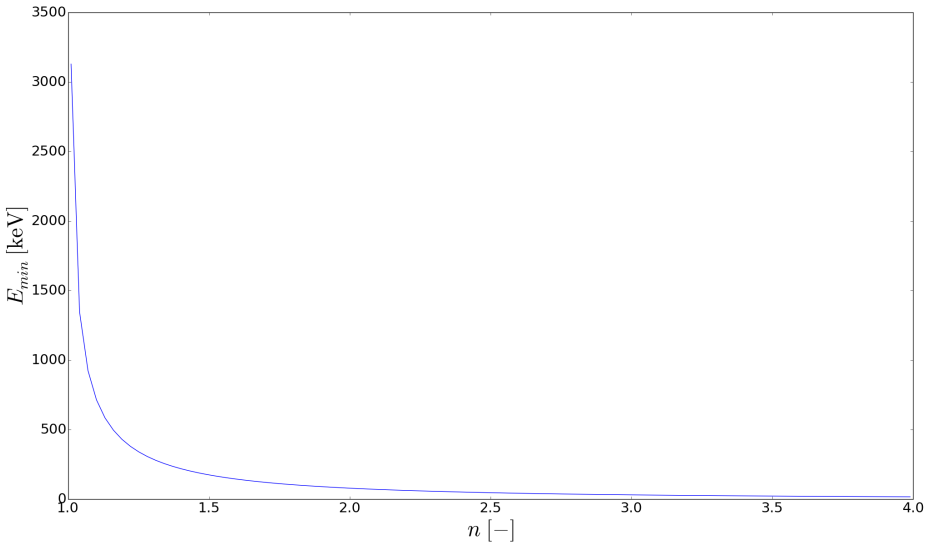

Figure 2.3: The minimal energy E_{min} required for electron to emit the Cherenkov radiation according to refractive index n of medium.

$$E_{min} = E_o\left(\frac{n}{\sqrt{n^2-1}} - 1\right), \tag{2.2}$$

where E_0 is rest energy of the particle. For example for electron $E_0^e = 511$ keV and for deuterium $E_0^d = 1863$ MeV. If we use the formula (2.2) to calculate the minimal energy required to emit the Cherenkov radiation for electron and deuterium in the water with refractive index $n = 1.33$, we get for electron $E_{min}^e = 264$ keV and for deuterium $E_{min}^d = 962$ MeV. Their velocities have to be greater than $0.76c$. In the Fig. 2.3, it is shown the dependence of minimal energy E_{min} on the refractive index n for the electron.

The energy dW emitted per unit length by the particle per unit frequency range can be calculated by the Frank-Tamm formula [24], which is given by

$$\frac{\partial^2 W}{\partial x \partial \omega} = \frac{q^2}{c^2}\omega\left(1 - \frac{1}{n^2(\omega)\beta^2}\right), \tag{2.3}$$

where q is the charge of travelling particle, ω is the frequency of emitted radiation and $n(\omega)$ is the frequency-dependent refractive index of the medium. The total amount of energy radiated by particle through Cherenkov radiation per unit length can be calculated using

$$\frac{\mathrm{d}W}{\mathrm{d}x} = \frac{q^2}{c^2}\int_{\beta n(\omega)>1} \omega\left(1 - \frac{1}{n^2(\omega)\beta^2}\right)\mathrm{d}\omega. \tag{2.4}$$

This integral is enumerated only over frequencies ω, which satisfy the condition $\beta n(\omega) > 1$. This meas that the particle travels in medium with greater velocity than the phase velocity of the light. The integral (2.4) is finite because the refractive index becomes unity at high frequencies. The formulas mentioned above can be also expressed in the wavelength λ of emitted radiation instead of frequency of emitted radiation ω by

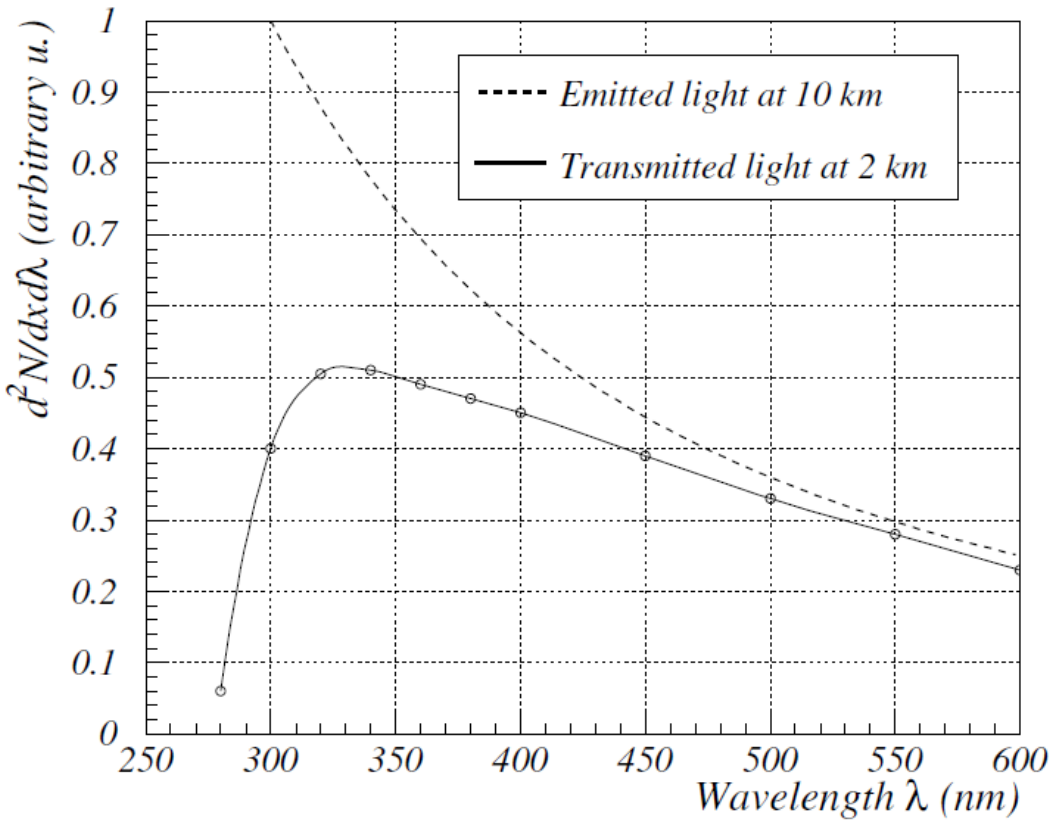

Figure 2.4: Example of the Cherenkov emission spectrum, compared to the spectrum after interacting with atmosphere. [25]

$$\frac{\partial^2 W}{\partial x \partial \lambda} = \frac{4\pi^2 q^2}{\lambda^3}\left(1 - \frac{1}{n^2(\lambda)\beta^2}\right), \quad \frac{\mathrm{d}W}{\mathrm{d}x} = 4\pi^2 q^2 \int_{\beta n(\omega)>1} \frac{1}{\lambda^3}\left(1 - \frac{1}{n^2(\lambda)\beta^2}\right)\mathrm{d}\omega. \tag{2.5}$$

2.2 Application of Cherenkov radiation

Some features of Cherenkov radiation can be used to inspect properties of the particle creating the Cherenkov light. The Cherenkov radiation is emitted only when particles moves in medium with given refractive index n with velocity greater than phase velocity. We can use this fact and construct the detector from materials with different n and then measure Cherenkov radiation. From this measurement we know the smallest possible velocity of the particle. The trajectory of the particle in the crystal can be derived from measurement of the cone axis direction. If we can deduce the Cherenkov angle θ_c, we will know something about particle energy. Furthermore If we are able to independently measure energy or momentum of particle, we will determined - with known θ_c - the mass of particle. On this principle for particle identification is based Ring Imaging Cherenkov Detectors (RICH).

Chapter 3

Cherenkov-type detector

Detection of relativistic electrons and measurements of their properties are important problems in the plasma fusion devices. Commonly, high-energy electrons are measured with the hard x-ray and neutron detector in tokamaks. These techniques are indirect, because they are focused on measuring secondary radiation or so called photoneutrons, which are caused by interaction of runaway electrons with limiter or the first wall of tokamak. One of the direct methods of measuring supra-thermal electrons in tokamak plasma is the Cherenkov-type detector. This chapter will deal with this of type detector and with its results.

3.1 Cherenkov detector

The Cherenkov detector, which is used in fusion devices, is based on the basic property of the Cherenkov radiation, namely on that particle moving at the greater speed than is the phase velocity of the light emit Cherenkov radiation. With the knowledge of this property of Cherenkov radiation and with the right choice of medium, we can build a simple threshold detector. Particles moving faster than light in the dielectric medium emit radiation and thus we can detect them.

3.1.1 Description of the detector

Single-channel detector based on Cherenkov effect is shown in the Fig. 3.1. As you can see the Cherenkov-type detector looks like a probe similarly to probes used in the studies of plasma edge. This type of detector can be placed in the radial or vertical port of the tokamak and due to the movable console can be inserted to the particular position in the vacuum chamber. The detector consists of a detecting head, a thin-wall metal tube and a cable of optical fibers. The measuring head of the detector consist of the radiator protected by a thin layer. The radiator is typically a crystal, which has a desired refractive index n. Detected particles are emitting radiation in this crystal. The radiators are covered by a thin layer of metal because of protection from the light and for additional setting of threshold energy of the detector. In the case of the detector, which is shown in the Fig. 3.1, aluminum nitride (AIN) is used as the radiator. This material has a refractive index of about 2.12. For electrons, the threshold energy is approximately 66 keV. However, the threshold energy of the detector for the electrons is not given only by the threshold energy of the radiator, but also by the thickness of the metal layer. For the single channel detector shown in the Fig. 3.1, the threshold energy is increased roughly to 80 keV due to metal coating. The Cherenkov radiation is transmitted from the radiator through a metal tube to a connector of the fiber cable at the other end of the tube. The Cherenkov radiation is transmitted through the optical

cable to a photomultiplier. The photomultiplier is usually shielded by lead bricks in order to protect the photo-cathodes against detrimental effect of possible hard x-ray noise.

To extend the measuring capabilities and to measure the fast electron populations with different energies, the multichannel Cherenkov detector was developed. Examples of different 4-channel Cherenkov detecting heads are shown in the Fig. 3.2. The detectors heads are equipped with four radiators made of AIN, each with diameter of 10 mm and 1 mm in thickness. The radiators are separated by stainless steel plates and mounted in a stainless steel box. All radiators have a small transparent window in order to enable optical contact with the optical cables to transport the detected emission to the photomultipliers. The version C is the most optimized and the final version of the measuring head.

The multi-channel Cherenkov detector has one disadvantage. The measuring sensitivity of the 4-channel detecting head was observed to be significantly decreased since the collecting surface of each detector is limited and is much smaller than the collecting surface of the single channel detector. This resulted in a strong decrease of the output signal [26]. The Cherenkov detectors were used in several fusion devices with minor changes in the design, but all detectors have same basic properties that were described above.

3.2 Former experiments with Cherenkov detector

The Cherenkov detector was first used in pulsed power plasma experiments, i. e. plasma focus and Z-pinch devices [27, 28]. Than authors of the detector proposed to adapt the detector to magnetic confinement fusion facilities [29]. In this section we will discuss experiments with runaway electrons involving the use of the Cherenkov detector on several devices.

3.2.1 CASTOR

The CASTOR tokamak was a small tokamak with the major radius of 40 cm, the minor radius of 10 cm and the limiter position at 8.5 cm. The toroidal magnetic field was ranging from 0.8 T to 1.4 T and plasma current varied from the 5 kA to 15 kA. The CASTOR tokamak could reach relatively low densities approximately in range $0.5 - 1.5 \cdot 10^{19}$ m^{-3}. Operation of the CASTOR tokamak ended in 2006 and then it was transported to the Faculty of Nuclear sciences and Physical Engineering of the Czech Technical University, where it serves under a name GOLEM for education of students.

In the first experiments on the CASTOR tokamak, it was observed [30] that intense Cherenkov signals appear particularly during the final phase of the tokamak discharge, probably when the expanding plasma column reaches the Cherenkov detector. The averaged values of the Cherenkov signal showed the dependence on the radial position of the Cherenkov detecting head and signals have significantly increased on the radial position which corresponds to the plasma confinement region. On the other hand, experimental data with additional tests showed a relatively strong influence of hard x-ray radiation on Cherenkov radiator and optical components of the detector.

With a new modified version of the Cherenkov detection system, it was possible to eliminate influence of hard x-rays on the photomultiplier [31]. In experiments on CASTOR tokamak detector with detecting head almost same as in Fig. 3.1 was used. The detecting head with this design allows change of the orientation of the detector input. Additional measurements with the Cherenkov detector head turned around its axis by 180° were also performed. The signals in the so called ion-side were negligible. These measurements confirm that the signals are induced by electrons and not by secondary x-rays. The values of the integrated Cherenkov signals, which are proportional to electron fluency, depended approximately linearly on the plasma current I_p [32].

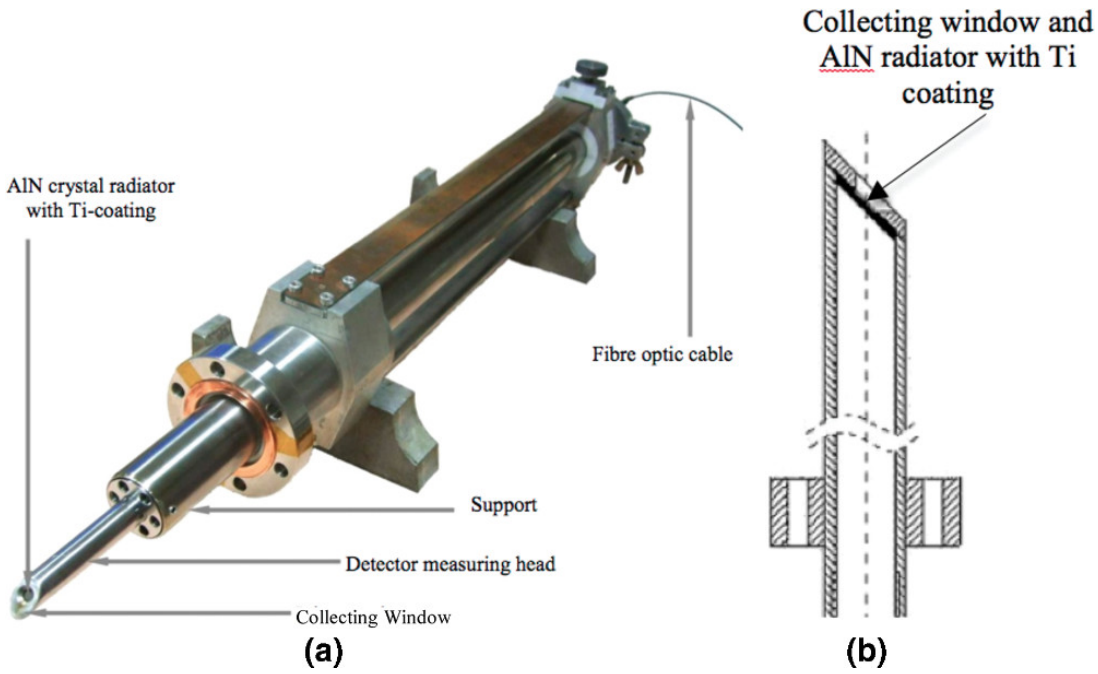

Figure 3.1: Single channel detector of electrons via Cherenkov radiation. (a) General view of the probe with vacuum flange and movable console. (b) Design of the detecting head. [26]

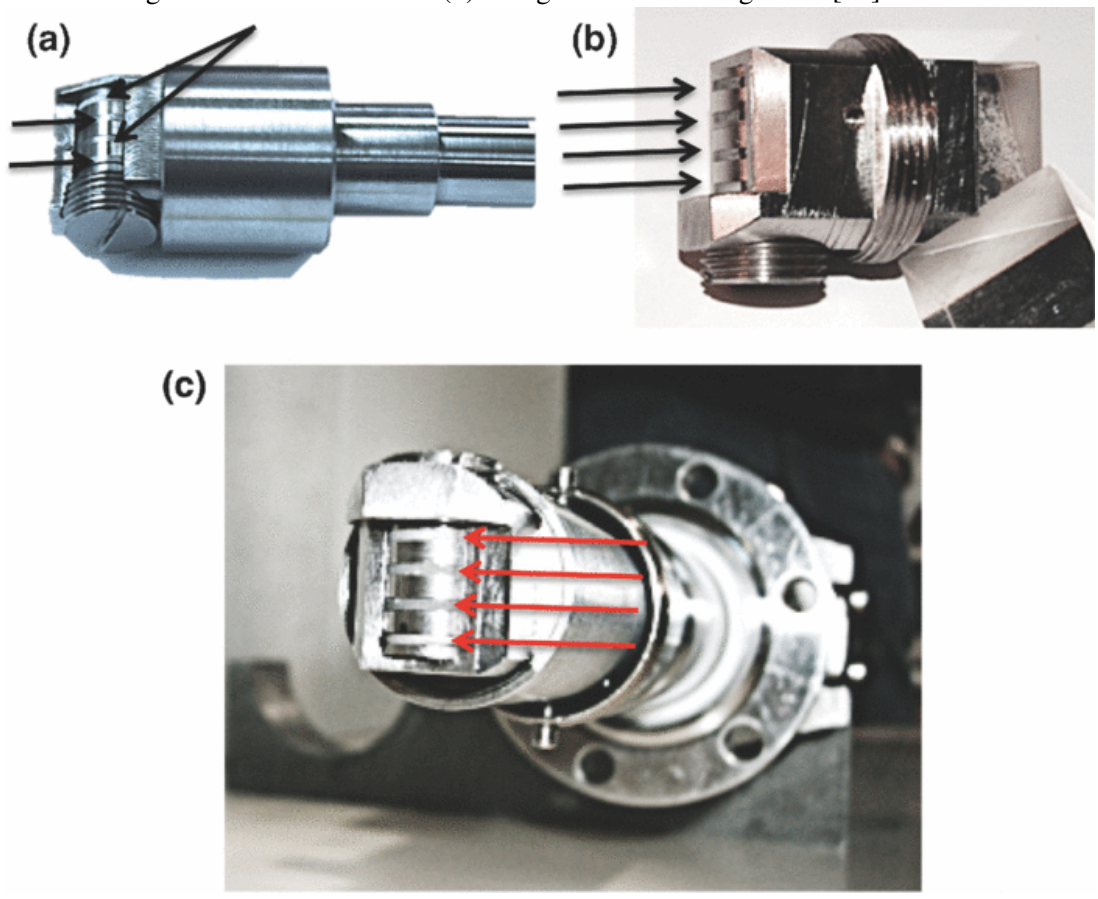

Figure 3.2: Details of four channel detector head. [26]

It can be concluded that appropriate Cherenkov detectors might be applied for investigation of fast electrons in other tokamak-type facilities.

3.2.2 ISSTOK

ISSTOK is a small size limiter tokamak with a circular plasma cross section. Major radius of the ISSTOK tokamak is 0.46 m, minor radius is 8.5 cm. A burst of the Cherenkov emission was observed at the beginning of the discharges in the ISTTOK tokamak. It signifies that at the beginning of the discharge there must be sufficiently high electric field and low density so that runaway electrons can be produced. In the first experiments on the ISSTOK tokamak only one channel Cherenkov detector was used and radiator was made of AIN and covered by titanium filter. This detector was able to detect electrons with energies above 80 keV. Using this type of Cherenkov detector, the runaway generation regime has been identified in the low current ISSTOK discharges. This result confirms the previous results obtained by numerical simulations [33, 34].

To determine the fast electrons fluence, the Cherenkov detector signals were integrated and compared for different tokamak regimes. As it was expected, the total fluence of the electrons decreased with the increase in the neutral hydrogen pressure for various plasma configuration. The measurements on the different radial position were also done.

In order to develop a diagnostic technique capable of characterizing fast electron populations with different energies, a prototype of a four-channel detector with molybdenum filters of different thicknesses has been designed and tested [35, 36]. Characterization of AIN radiator with different thickness of Mo-filters has been carried out on a special test stand. In this stand, a electron beam generated by a linear accelerator has been used. The energy of the electrons in the beam was 6 MeV, which is well above detecting threshold of the AIN radiator (66 keV).

The radiators of the Cherenkov detector were 10 mm in diameter and 1 mm thick. The collection surface of each channel was only about 3 mm^2, which is less than in the first experiments. This resulted in the decrease of the amplitude of the recorded signals. The temporal evolution of the measured signals showed the close correlation between all channels. In fact all registered signals were almost of the same value.

3.2.3 TORE SUPRA

For the measurements performed on the TORE SUPRA tokamak diamond crystals were selected as radiators. Diamond crystal is characterized by the relatively low threshold for production of Cherenkov radiation (51 keV), but high thermal conductivity. In order to reduce overheating of the Mo and diamond radiators it was proposed to fix the Cherenkov measuring head on the movable shaft, which can be inserted into plasma region and removed again within a few tens of milliseconds [37].

The designed and manufactured measuring head contained four diamond radiators with different thickness of Mo layers. The threshold energies of four channels of the Cherenkov detector were 84, 109, 173 and 259 keV . The whole head was protected by a cylindrical shielding made of CFC, and only four tips of the diamond radiators were available from outside. The head of the Cherenkov detector is shown in the Fig. 3.3. In all the cases the Cherenkov measuring head was moved along the tokamak minor radius into the scrape-off layer to the deepest positions, in which the top of the probe was placed 80 – 100 mm outside LCFS.

The measurements on the TORE SUPRA tokamak were the first measurements with the Cherenkov detector, which were done in a large tokamak experiment. The measuring head was mounted on the reciprocating probe. Preliminary results suggested that a thin sheath of fast electrons might be observed if a level of the LH heating is high enough.

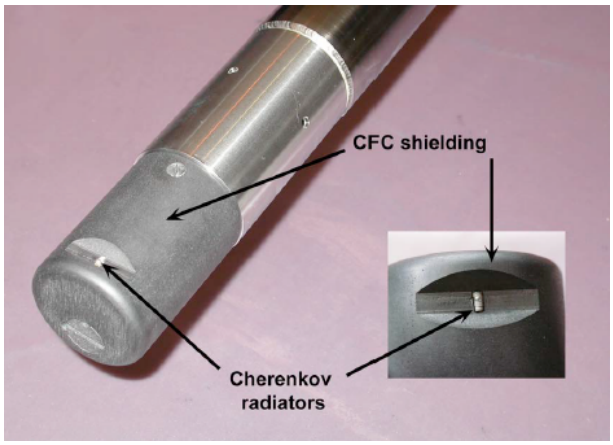

Figure 3.3: Picture of the Cherenkov measuring head equipped with four diamond radiators, which was constructed for TORE-SUPRA. [37]

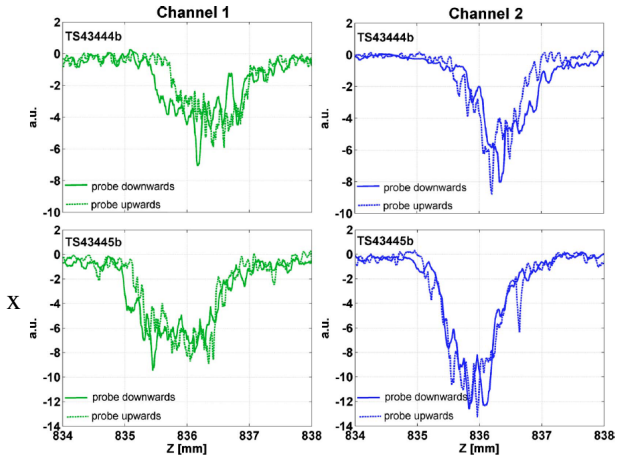

Figure 3.4: Signals of Cherenkov radiation obtained from two measuring channels during second probe insertions for two successive shots. [37]

The appearance of the streams of fast electrons was deduced from previous probe measurements and damages of diagnostics ports. In fact electron-induced Cherenkov signals were recorded in the shots, when LH heating was applied to plasma. It should be pointed out that during ohmic discharges, where no electrons losses were expected, no signals were recorded. The recorded signals of the Cherenkov radiation from two shots are shown in the Fig. 3.4. In the Fig. 3.4 you can see data from channel 1 ($W_e > 84$ keV) and channel 2 ($W_e > 109$ keV) from shots TS43444 and TS43445. Other remaining channels are not shown, because they did not delivered any distinct Cherenkov signal. The lack of the signal from channel 3 ($W_e > 173$ keV) and ($W_e > 256$ keV) can be explained by the lack of electrons with energies greater than 173 keV or by shadowing of radiators corresponding to the channel 3 and 4.

In the next experimental campaign new prototype of the Cherenkov detector was used. The main difference from previous version was the placement of the Cherenkov radiators at the top of the probe to eliminate any shadowing. The previous design and the new design of the Cherenkov head are shown in the Fig. 3.5 and Fig. 3.6. The most distinct differences between results obtained by the old version of the Cherenkov detector and the new one were changes in shapes of signals and substantial increase of the intensities of recorded signals. An analysis of signals recorded by new version of the Cherenkov head showed that in the scrape off layer there were no thin electron streams [38], which were suspected on the basis of the preliminary measurements performed earlier. Measurements showed the presence of a large zone of constant flux of electrons.

3.2.4 FTU

FTU is a compact, high field tokamak, with a major radius 0.935 m a minor radius 0.33 m. The single channel Cherenkov detector was successfully installed and Cherenkov detecting head was placed in the shadow of the limiter. Signal from the Cherenkov detector was found correlated with other signals, i. e. Mirnov coils, ECE, soft x-rays, gamma and neutron detector. From the analyses of the recorded data can be deduced that the Cherenkov signal occur when the O-point of the the island faces the probe. The signal vanishes when the O-point moves away from probe. RE emission is in those cases dominated by the island rotation. This confirm that one of mechanism of RE expulsion is the interaction of the runaway electrons with the magnetic perturbation due to the island. The intensity of the Cherenkov signals was found to be linearly proportional to the gamma ray rate [39].

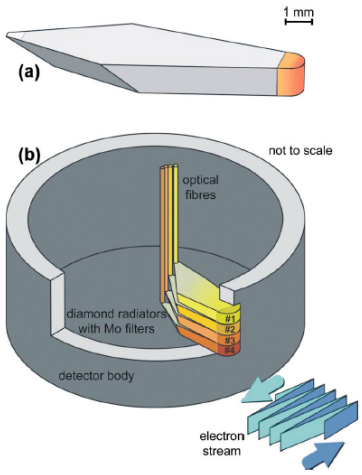

Figure 3.5: (a) Single diamond radiator design for the Tore Supra experiments. (b) The spatial arrangement of four diamond radiators and separate optical fibers of four-channel Cherenkov detector.

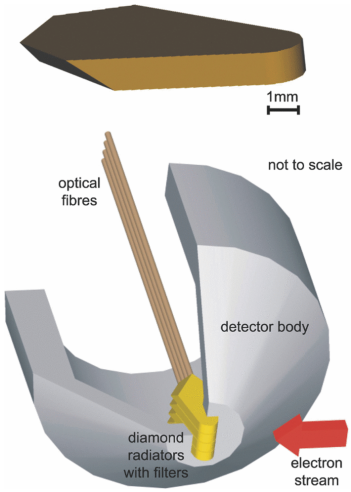

Figure 3.6: Picture of the modified diamond radiator (top) and a schematic drawing of the modified Cherenkov measuring head (bottom).

3.2.5 COMPPASS

First tests of Cherenkov detector in COMPASS tokamak were carried out in 2012. A prototype of the single-channel Cherenkov measuring head, equipped with a radiator made from AIN, was manufactured and tested. During a short experimental session, measurements were conducted for several detecting-head positions along minor radius of the tokamak.

First experimental campaign focused on the study of runaway electrons with the use of Cherenkov detector took place in 2014. AIN crystal was used as a Cherenkov radiator with a diameter 10 mm and thickness of 1 mm. The collecting surface of the Cherenkov head was approximately 3 mm^2 and the energy threshold of the detected electrons was 70 keV. The detecting head was covered by a graphite protection. The detecting head of the Cherenkov detector with graphite armor and vacuum flange are shown in the Fig. 3.7. In the Fig. 3.8, you can see a complete set of measuring head together with a manual holder.

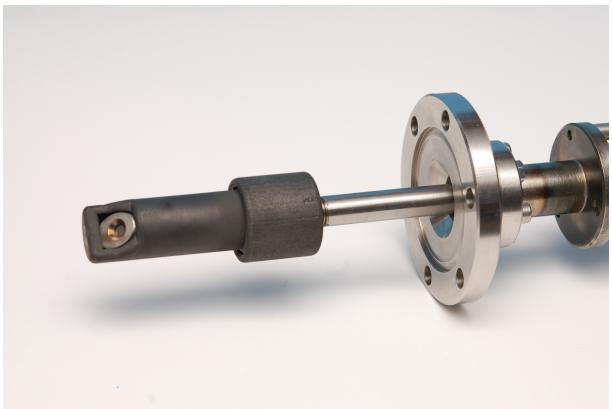

Figure 3.7: The detecting head of the Cherenkov detector with graphite armor and vacuum flange.

Figure 3.8: The Cherenkov probe with manual holder.

In the experimental campaign, which was held in the spring of 2015, the Cherenkov detector with new design was used. It was still single channel Cherenkov detector, but the radiator was placed on the top of the Cherenkov head, similarly as it is shown in the Fig. 3.6. As a radiator CVD diamond was used, which has refractive index 2.42 and the lowest energy threshold for the production of Cherenkov radiation for electron is 51 keV. The radiator was 8 mm in diameter, 1 mm in thickness and was covered by titanium, platinum and gold of thickness 100, 200 and 1000 nm respectively. Additional metal filters increased the detecting threshold energy to 58 keV. The described Cherenkov detector is shown in the Fig. 3.9.

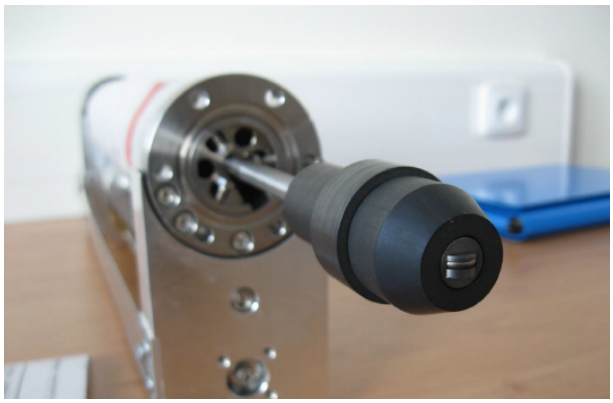

Figure 3.9: The detecting head of the Cherenkov detector with graphite armor and vacuum flange.

Figure 3.10: The Cherenkov probe with manual holder.

In the next experimental campaigns three-channel Cherenkov detector was used. The head of the Cherenkov detector is shown in the Fig. 3.10. The radiators were the same as in the previous version of Cherenkov detector and all radiators were covered by the same metal inter-layer as previous. Only channel 2 and channel 3 were covered by additional layer of molybdenum of thickness 35 μm and 77 μm respectively. The molybdenum layer was added to increase the energy threshold of each channel. The Cherenkov detector had the electron energy thresholds 58, 145 and 221 keV.

Chapter 4

Experimental results

In this chapter overview of used diagnostic tools important for the RE studies is given. Furthermore following chapter deals with the analyzing of experimental data, which were measured during RE experiments on tokamak COMPASS.

4.1 Experimental setup

Experimental setup, which was used during runaway electrons experiments, is shown in the Fig. 4.1. The interaction of the runaway electrons with plasma facing components (PFC) leads to the emission of hard x-ray radiation. This resulting hard x-ray radiation (HXR) is measured on tokamak COMPASS by scintillation detector. The detector is based on a photomultiplier combined with NaI(Tl) scintillator. The hard x-ray detector is situated in the north of the tokamak hall. To measure HXR is additionally installed second scintillation detector, which is borrow from FNSPE CTU. Signals from standard and borrowed

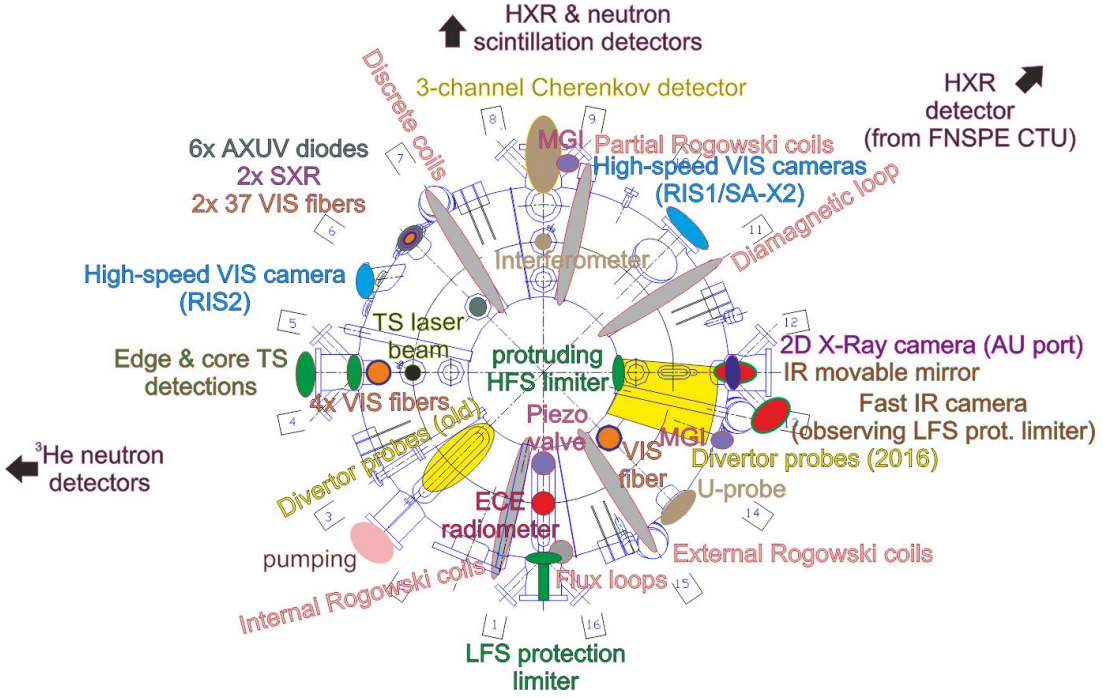

Figure 4.1: Experimental setup used during runaway electrons studies.

hard x-ray detector will be in the following text denoted as HXR and HXR2 respectively. The so called photo-neutrons, which are produced by interaction of high energetic RE with wall, are measured by plastic scintillation detector. The neutron detector (HXR-S) is placed inside the lead housing (10 cm) in the north of the tokamak hall near the standard HXR detector. It was shown that this detector is also sensitive to the high energy photons ($1 - 10$ MeV). Furthermore the tokamak COMPASS is equipped by two ^{3}He neutron detectors, which are located next to the west wall of the tokamak hall.

The Cherenkov detector described in the previous chapter is located in the horizontal port of the tokamak on the mid-plane. This detector is approximately on the same toroidal position as the HXR and neutron detectors. The Cherenkov detector is placed on the movable support, which enable to put the detectors measuring head on the particular radial position. The Cherenkov detector and its movable support installed on the Compass tokamak is shown in the Fig. 4.2. From the Cherenkov detector induced radiation is transmitted through the optical cables to the photomultipliers, which are situated in

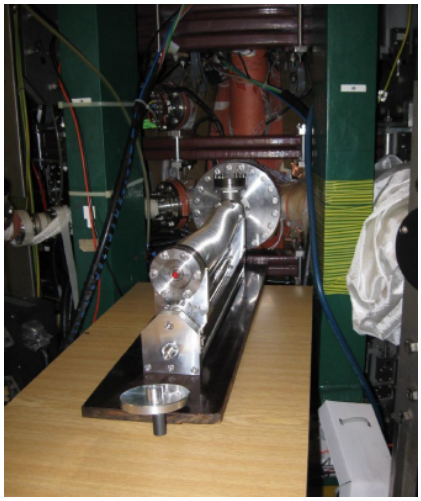

Figure 4.2: Location of the Cherenkov detector in the horizontal port on the mid-plane of tokamak.

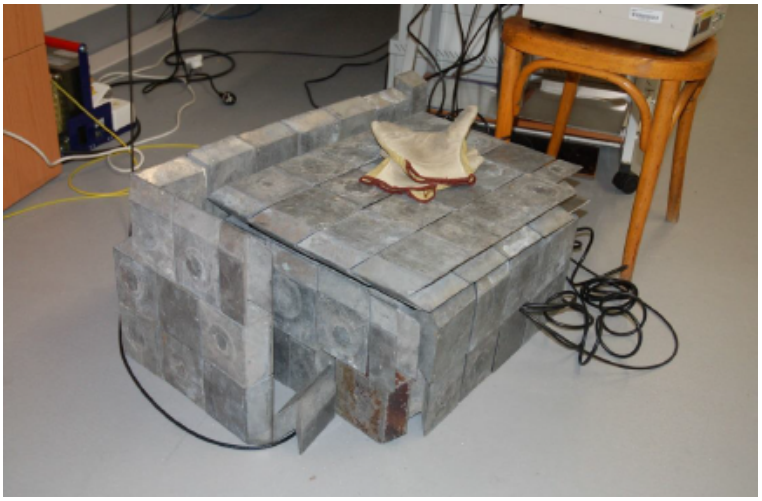

Figure 4.3: Lead box 15 cm in thickness built in the next room from the tokamak hall protecting the photomultipliers of the Cherenkov detector against HXR radiation.

the next room from the tokamak hall. Furthermore the photomultipliers are placed in the lead box 15 cm in thickness because of its protection against hard x-ray radiation. To monitor level of HXR radiation in the lead box a scintillation detector (XET) is placed there. Lead box protecting photomultipliers is shown in the Fig. 4.3. Signals from first, second and third channel of the Cherenkov detector will be in the following text denoted as CH1, CH2, CH3 respectively.

Two fast cameras with advanced features for fusion research are installed for purposed of visible light observation of the plasma discharge. Cameras can give important information about evolution of plasma discharge and provide a evidence about existence of runaway electron beam. High speed cameras are situated on the different toroidal position of the tokamak. One of cameras is placed in tangential port with a variable mechanical holder.

To trigger disruption and create a runaway electron beam massive gas injection (MGI) valves are used. These valves can release a large amounts of gas and thus terminate a discharge. For termination of a discharge noble gases as argon or neon are used. The tokamak COMPASS have two MGI (north, west) valve available.

For protection of diagnostics and tokamak itself the movable low-field side protection limiter is installed before each runaway electron campaign. The protection limiter is placed on the mid-plane and

the radial position of the edge of the protection limiter is 760 mm. It has to be mentioned, that the Cherenkov detector is for safety always operated only in the shadow of the limiter.

4.2 Different RE regimes

Runaway electron regimes on COMPASS tokamak are strongly sensitive on small changes of plasma parameters and tokamak setup. In the Fig. 4.4 are shown basic plasma properties for three almost similar discharges on tokamak COMPASS. Evolution of the plasma current I_p and loop voltage U_l are approximately same for all three discharges, but the evolution of the electron density n_e slightly differs during the discharge.

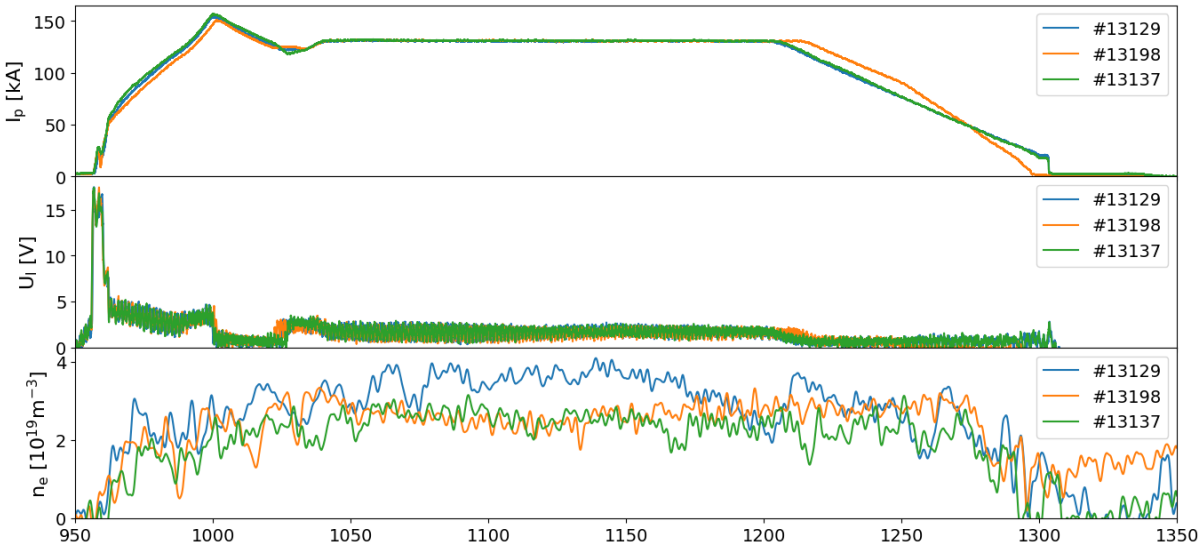

Figure 4.4: Comparison of three almost similar shots on the COMPASS tokamak .

Despite the fact that basic plasma parameters evolve nearly similar, RE regimes differ significantly. It can be seen in the Fig. 4.5. In this figure are shown signals from hard x-ray detector, neutron detector and from first channel of the Cherenkov detector. The first RE regime (#13129) is characterized almost by none production of the HXR radiation. Signals from neutron and the Cherenkov detector shows zero during the whole discharge. The second RE regime (#13198) is characterized by production of HXR radiation during whole discharge and the detector is saturated on he same level from the beginning to the end of the shot. In this case we can see that signal from neutron and Cherenkov detector appear during the discharge. Appearance of the signal from first channel of Cherenkov detector suggests presence of electrons with energies higher than 58 keV. Evidence of even energetic electrons is non-zero signal from the neutron detector. The energetic thresholds for production of so called photo-neutrons in reactions D(γ,n)H, ^{13}C(γ,n)^{12}C and ^{56}Fe(γ,n)^{55}Fe are 2.2 MeV, 18.7 MeV and 11.2 MeV respectively. But we have to have in mind, that neutron detector is despite its led shielding sensitive to the high energetic photons to. The third RE regime (#13137) is characterized by relatively strong HXR radiation in the beginning of the discharge and decreasing magnitude of the intensity of the signal during the shot. Signals from neutron and the Cherenkov detector are weak in this case.

The Fig. 4.5 shows that the evolution of the signal from Cherenkov detector has similar properties as the signal from neutron detector, although the energetic threshold for detection substantially differs. The Cherenkov radiation is induced by electrons with energies higher than 58 keV, but the radiation

or neutrons detected by neutron detector are produced by electrons with energies of three orders in magnitude higher (MeV). This fact can be explained at least in two ways. The Cherenkov detector is sensitive to high energetic photons and induced radiation is not caused by propagating electrons through detectors head or incoming photon can undergo Compton scattering and create electron, which can gain enough energy to emit Cherenkov radiation in the detector. On the other hand, similarities between signals can be explained completely different and so that only electrons with relatively high energies (MeV) can reach a Cherenkov measuring head. The less energetic electrons can not reach the detector and impact to the limiter and cause HXR radiation.

For the future analysis has to be mentioned, that the radial position of the Cherenkov head was 775 mm and the voltage on power sources of photomultipliers was 1.6 kV.

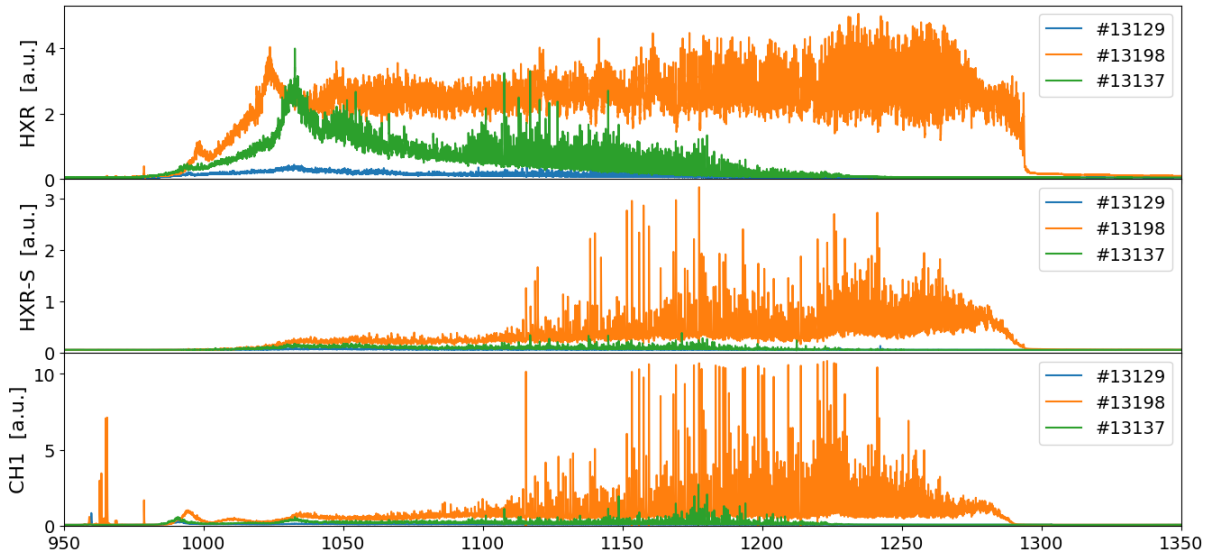

Figure 4.5: Comparison of signals from HXR detector (HXR), from neutron detector (HXR-S) and from first channel of Cherenkov detector (CH1) to demonstration of different RE regimes.

4.3 Radial position scan

Very useful and important experiment for better understanding of runaway electron physics and to verify functionality of the detector is radial position scan of induced Cherenkov radiation. The idea of this experiment is simple and consists of a gradual insertion of the Cherenkov detector head along minor radius of the tokamak. One of the difficulties is that this radial scan have to be carrying out on shot to shot basis. It requires very good repeatability of discharges including their RE regime.

I_p^{ft} [kA]	n_e [10^{19}m^3]	B_T [T]	T_e [keV]	plasma shape
130	3.3	1.15	≈ 1	circular

Table 4.1: Basic parameters of the discharges in the radial position scan of induced Cherenkov radiation. I_p^{ft} denotes plasma current during the flat-top. n_e is density of electrons. B_T and T_e denote magnetic toroidal field and electron temperature respectively.

In the Fig. 4.6 one discharge (#14563) from radial position scan is shown for illustration. Basic parameters of the discharges are summarize in the Tab. 4.1. As can be seen in the Fig. 4.6 signal from

HXR detector is visible almost during the whole discharge, but is not saturated on the same level, which suggests relatively small losses of the runaway electrons. Signal from neutron detector is very weak. Radial position scan was done in the five different position along minor radius of tokamak. The deepest position was R = 763 mm, which is 3 mm behind the edge of the protection limiter. As was mentioned before, the Cherenkov detector measurement head was due to safety reasons operated only in the shadow of the limiter to prevent the overheating detector. During all experiments the Cherenkov detector head was observed by the IR camera to monitor its temperature.

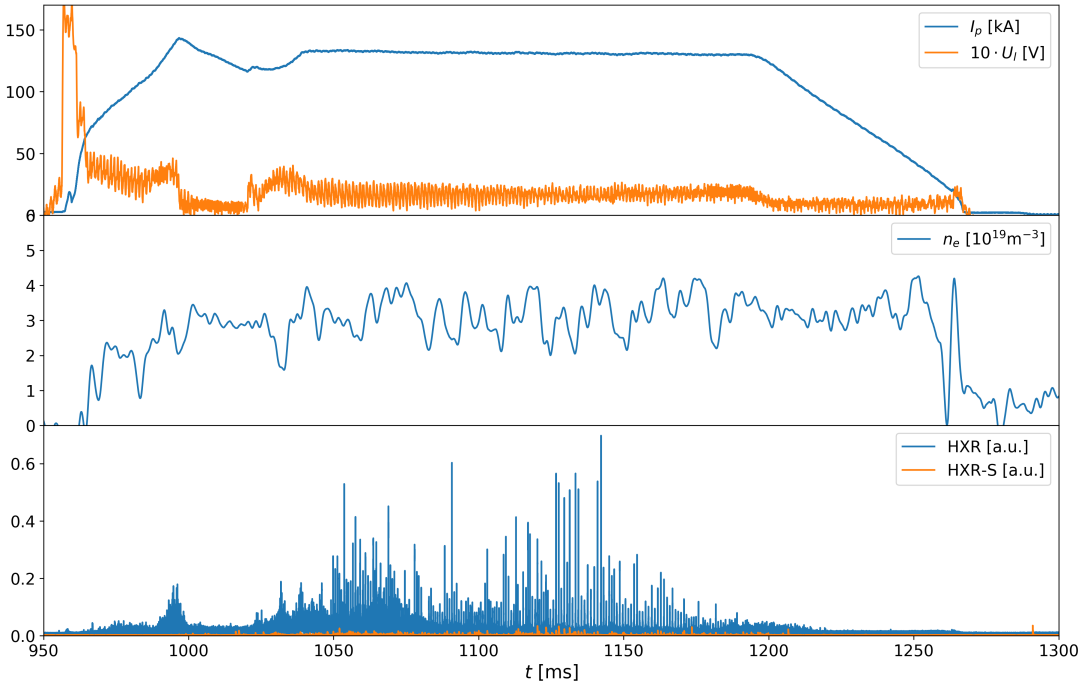

Figure 4.6: Evolution of basic parameters of the discharge #14563.

Evolution of the signals from all channels of Cherenkov detector from the radial position scan are shown in the Fig. 4.7. All five shots were done with same setting of voltage on the power supplies of photomultipliers belong to Cherenkov detector and thus we can easily compare measurements, which were carried out on different radial positions. Numbers of shots and settings of the Cherenkov detector during the position scan are displayed in the Tab. 4.2. As can be seen from the first picture on the Fig.

Shot	#14558	#14559	#14560	#14562	#14563
R [mm]	780	770	767	765	763
U_{PS} [kV]	1.6	1.6	1.6	1.6	1.6

Table 4.2: Setting of Cherenkov detector during the radial position scan. R and U_{PS} denote radial position of Cherenkov detector and voltage on power sources of photomultipliers.

4.7, signal from the Cherenkov detector is almost zero during the whole discharge and appears only little bursts of signal from Cherenkov detector. With the gradually inserting of the detector deeper into the tokamak the signals from all channels rise up and achieve the highest possible value for substantially duration of the shot on the deepest radial position of the detector measuring head. If we assume that energy distribution of particles escaping from the plasma is uniform on spatial scale of the detector and

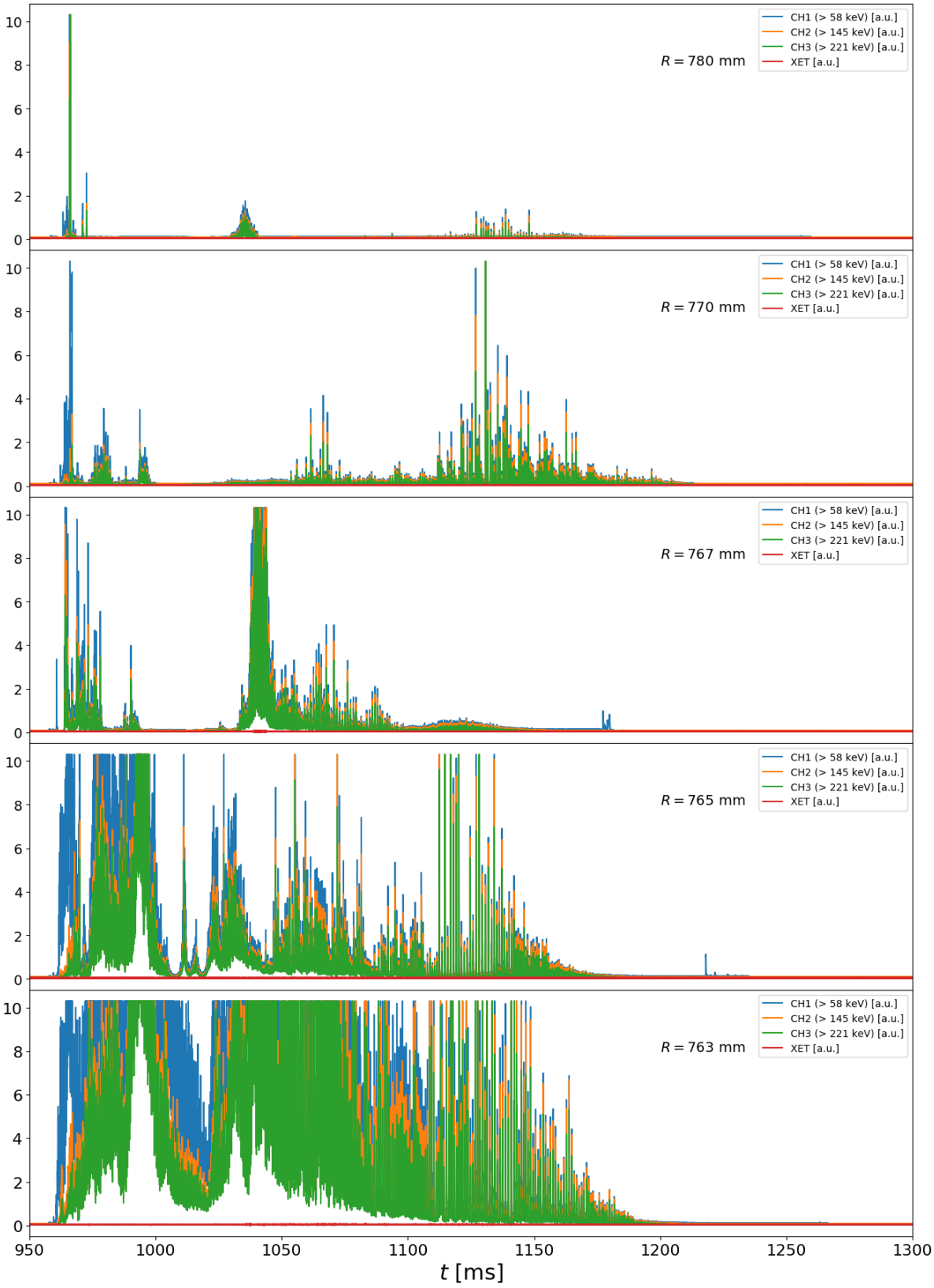

Figure 4.7: Evolution of the signals from the first (CH1), second (CH2) and third (CH3) channel of the Cherenkov detector. In this figure are displayed signals from shots #14558, #14559, #14560, #14562 and #14563 respectively.

efficiency of the each channel is roughly same, we can investigate energy distribution of the particles on different radial position. The intensity of the signal from Cherenkov detector is proportional to the electron flow propagating through the Cherenkov detector measuring head. If we integrate the signal in the time domain, we get quantity, which is in literature often called electron fluency and in the following text will be denoted by the symbol $\int$CHX, where X represents number of the channel.

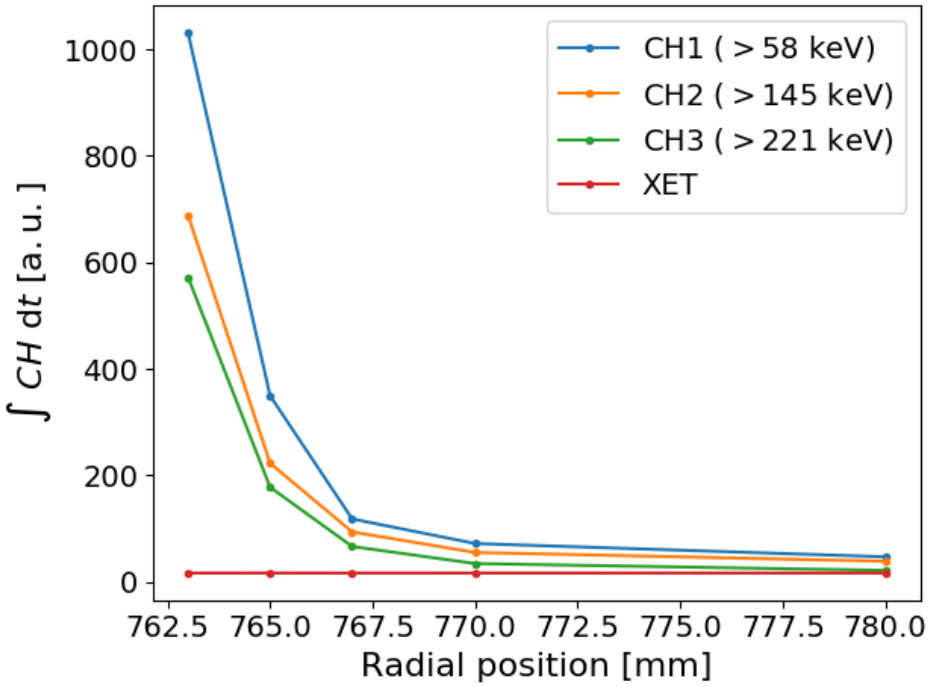

Figure 4.8: Radial profile of electron fluency $\int$CH (integral of the signal from Cherenkov detector in time domain). CH1, CH2 and CH3 denote signals from first, second and third channel of the Cherenkov detector. XET is the signal from the scintillation detector, which is placed in the led housing of photomultipliers belongs to the Cherenkov detector and monitors level of HXR radiation there.

Determined radial profile of electron fluency (integral of the signal from Cherenkov detector) is shown in the Fig. 4.8. As can be seen from this figure, the magnitude of the electron fluency is approximately same for all channels on the most outer position. With decreasing radial position, the electron fluency rise exponentially and differences between channels are increasing. In the Fig. 4.8 signal from scintillation detector is also display, which is located in the led housing of Cherenkovs photomultipliers. This detector monitors level of HXR radiation, which can influence right measurements with the Cherenkov detector. But we can see, that signal from XET is for all discharges on same level and is zero.

When we realize, that the electrons, which are detected by the third channel of the Cherenkov detector, should be detected by the first and second channel and further electrons detected by the second channel should be detected by first channel of the detector, we can determined relative population of the electrons in different energetic ranges. The first channel is able to detect electrons with energies higher than 58 keV and second channel detect electrons with energies from 145 keV, so if we subtract signal the second channel from the first, we get signal, which is caused by the electrons in energy range 58 – 145 keV. On the other hand, if we subtract the third channel from second channel, we get signal induced by electrons in energy range 145 – 221 keV. For the signal from third channel are responsible electrons with energies higher than 221 keV.

In the Fig. 4.9 we can see relative population of electrons in various energetic ranges on different radial position. From this figure it can be seen, that in outer position there are preferably particles with energies higher than 221 keV. With deeper insertion of the detector to the tokamak signals corresponding to the detection of electrons in energetic range 58 – 221 keV appear. But signal induced by electrons with energies from 221 keV dominates on all radial position of the detector.

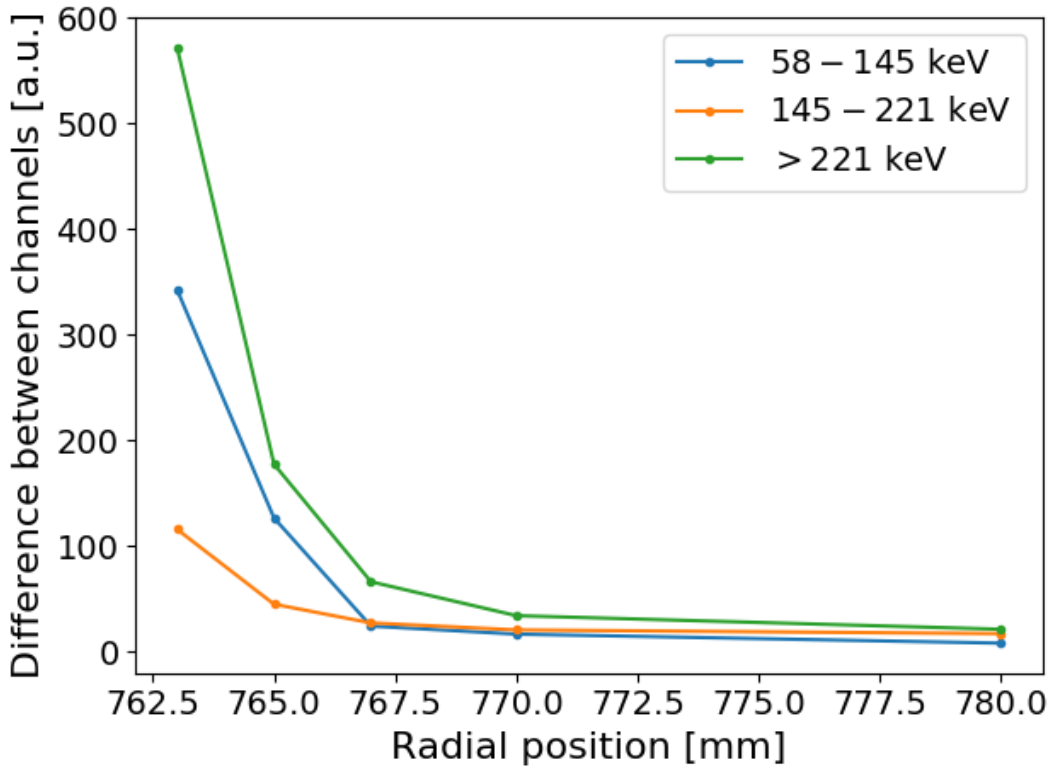

Figure 4.9: Difference between channels of the Cherenkov detector. These differences shows representation of individual energetic ranges of detected electrons on particular radial position.

One explanation of this feature of the Cherenkov detector position scan is, that only high energetic electrons can reach measuring head of the detector, when is placed deep in the shadow of the protection limiter ($R \geq 770$ mm). Less energetic electrons can not get on the radial position of the detector and impact to the protection limiter, when they escape from the plasma. For the illustration of this situation, you can see at Fig. 4.10. In this figure you can see very simplified drawing of the situation mentioned above. The Cherenkov detector and protection limiter are display there, together with trajectories of two electrons with different energies. The trajectory of electron with the greater energy is represented by the red curve. On the other hand, the trajectory of less energetic electron is marked by orange curve.

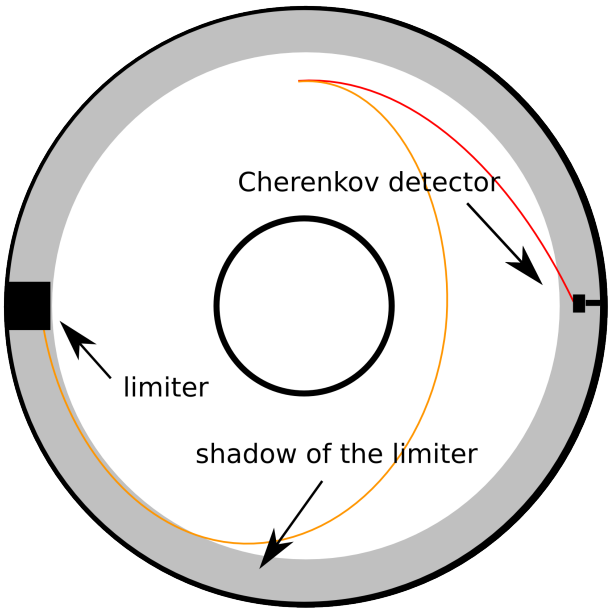

Figure 4.10: Illustration of the possible explanation of the experimental results from the radial position scan of the Cherenkov detector.

4.4 Post-disruption RE beams

One of the most important research related to runaway electron physics is investigation of runaway electron beams. The post-disruptive RE beam can be the most dangerous event for ITER. In the small or medium size tokamaks is difficult to produce RE beam during fast plasma termination. Rapid plasma termination of the plasma is achieved by the argon massive gas injection. Argon triggers thermal quench (sudden temperature drop) and thus cause the abrupt increase of the plasma resistivity, which leads to the rise of loop voltage. The hot-tail mechanism, described in the first chapter, apparently plays a significant role during creation of the RE beam.

4.4.1 Description of RE beams

As was sad above, for small tokamaks is difficult to produce RE beam by rapid plasma termination, but one way how to do it is argon injection in the current ramp-up phase. It was done on Tore Supra [40] and similar scenario was developed on COMPASS tokamak [40], but this scenario is not completely reliable. The typical evolution of the argon induced RE beam in the ramp-up current phase on COMPASS tokamak is shown in the Fig. 4.11. In the first graph plasma current I_p, loop voltage U_l and intensity of radiation of H_α line are displayed. Evolution of the signal from HXR detector (HXR) and neutron detector (HXR-S) are shown in the second graph. Signals from Cherenkov detector are in the third graph.

The massive gas injection valve was triggered in time 953 ms, but the response time of the valve is estimated to be around 10 ms. The time in which argon starts to flow into the chamber is thus approximately 963 ms. This time is marked in first graph as *Argon puff*. The first stage of the plasma termination, called thermal quench (*TQ*), occurs about 970 ms. This time can be estimated from ECE measurements and can be identified by sudden drop of ECE signal, which corresponds to the plasma temperature or by increase of intensity of plasma radiation suggesting plasma cooling. After the thermal quench phase follows current quench phase is characterized by the abrupt decrease of plasma current.

When the decreasing of plasma current stops, RE beam plateau phase starts. In this moment plasma current is completely carried by runaway electrons.

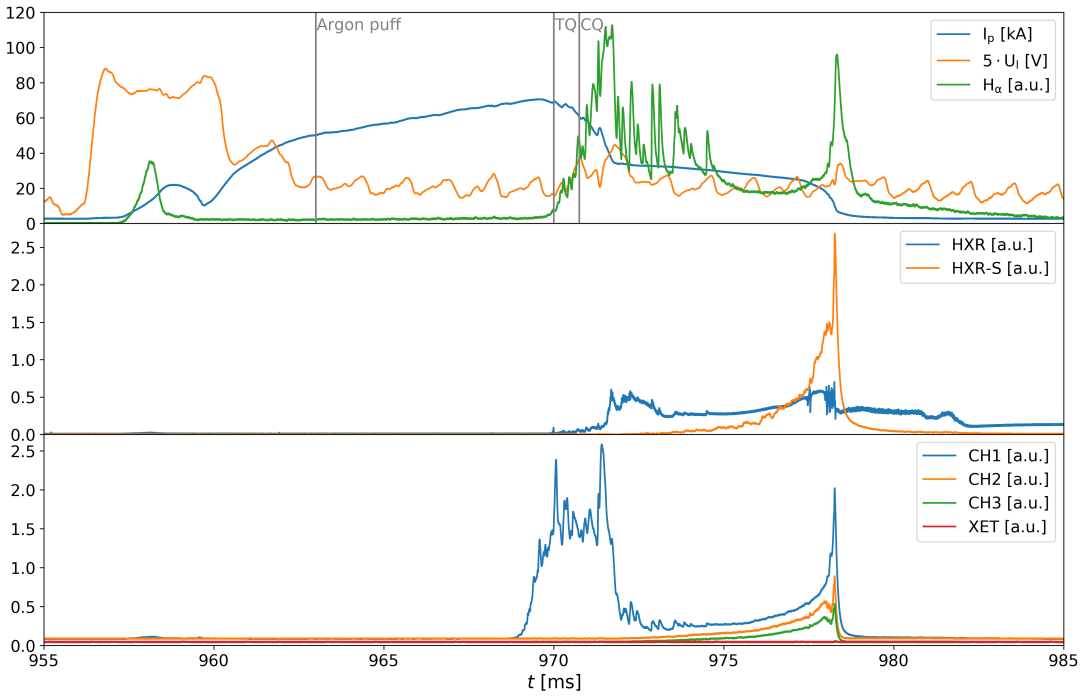

Figure 4.11: Evolution of the basic plasma parameters during induced Argon disruption with creation of RE beam (#13120).

Signal from HXR detector starts in the thermal quench phase and goes into the saturation, when RE beam is formed. Neutron signal appears in the beginning of the RE plateau and continuously rise in the next phase of the plasma discharge. During plasma disruption we can see strong burst of the induced Cherenkov radiation, which is detected by the first channel (CH1). Then intensity of the signal from the first channel decreases and again steadily grows in RE plateau phase and peaks in the end of the discharge. The signals from the second and third channels rise in the correlation with the signal from neutron detector. In Fig. 4.12, images from fast camera showing evolution of the plasma discharge and creation of RE beam are shown. In the second and third frame is clearly visible filamentary part of the creation of RE beam. This phenomenon was studied in [reference].

Signal from HXR detector starts in the thermal quench phase and goes into the saturation, when RE beam is formed. Neutron signal appears in the beginning of the RE plateau and continuously rise in the next phase of the plasma discharge. During plasma disruption we can see strong burst of the induced Cherenkov radiation, which is detected by the first channel (CH1). Then intensity of the signal from the first channel decreases and again steadily grows in RE plateau phase and peaks in the end of the discharge. The signals from the second and third channels rise in the correlation with the signal from neutron detector. In Fig. 4.12, images from fast camera showing evolution of the plasma discharge and creation of RE beam are shown. In the second and third frame is clearly visible filamentary part of the creation of RE beam. This phenomenon was studied in [41].

In the Fig.4.13 comparison of discharges #13118 and #13120 is shown. During the rapid termination of the plasma RE beam was not created in the discharge #13118, but the discharge #13120 represents the opposite situation. These two situation can be easily distinguished by evolution of signals from the

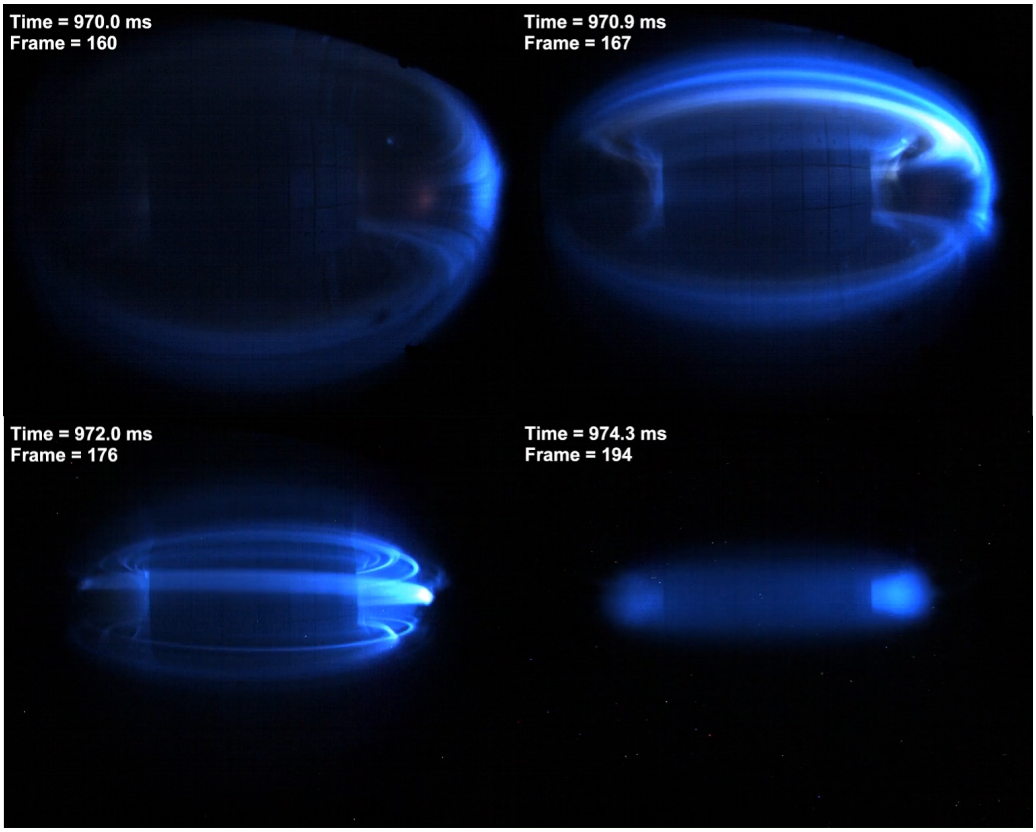

Figure 4.12: Images from the fast camera of shot #13120 showing evolution of the plasma discharge and creation of runaway electron beam.

Cherenkov detector. Both discharges are characterized by strong emission of the Cherenkov radiation during disruption recorded by first channel of Cherenkov detector, but in the case when RE beam is created, signals from all channels are gradually increasing until the end of the discharge. A similar situation to that described above is displayed in the second graph of the Fig. 4.13. Signals from HXR and neutrons detectors is shown there. Only short and very small burst of HXR radiation is recorded during disruption in the discharge #13118 and signal from neutron detector is zero all the time. In the discharge #13120 HXR detector has the strong signal from the moment of disruption and goes to saturation during RE beam plateau phase. One of the reasons why the RE beam is not created during the discharge #13118 is that the plasma was the radially unstable immediately after disruption and drifts to the HFS ans hits the central column. In case of RE beam creation (#13120) plasma also drifts to the HFS, but with the creation of the RE beam starts to move in the opposite direction to the LFS. Movement of RE beam to the LFS is accompanied by radial expansion of RE beam.

In Fig. 4.14, evolution of discharge #10921 is shown. This discharge is from the campaign, which was held in 2015. During this experimental campaign the three-channel Cherenkov detector was also used, but was located on the movable support, which did not allow insert the detection head of the Cherenkov detector sufficiently into the vacuum chamber. The most deepest position was 784 mm that means it was possible to placed the detector 6 mm in front of the chamber, i. e. 24 mm behind the protection limiter. During this discharge was also applied rezistor to decrease amplitudes of signals from the Cherenkov detector. This changes of setting of the Cherenkov detector result in absolutely different evolution of signals. If we compare evolution of signals displayed in Fig. 4.11 and Fig. 4.14, we

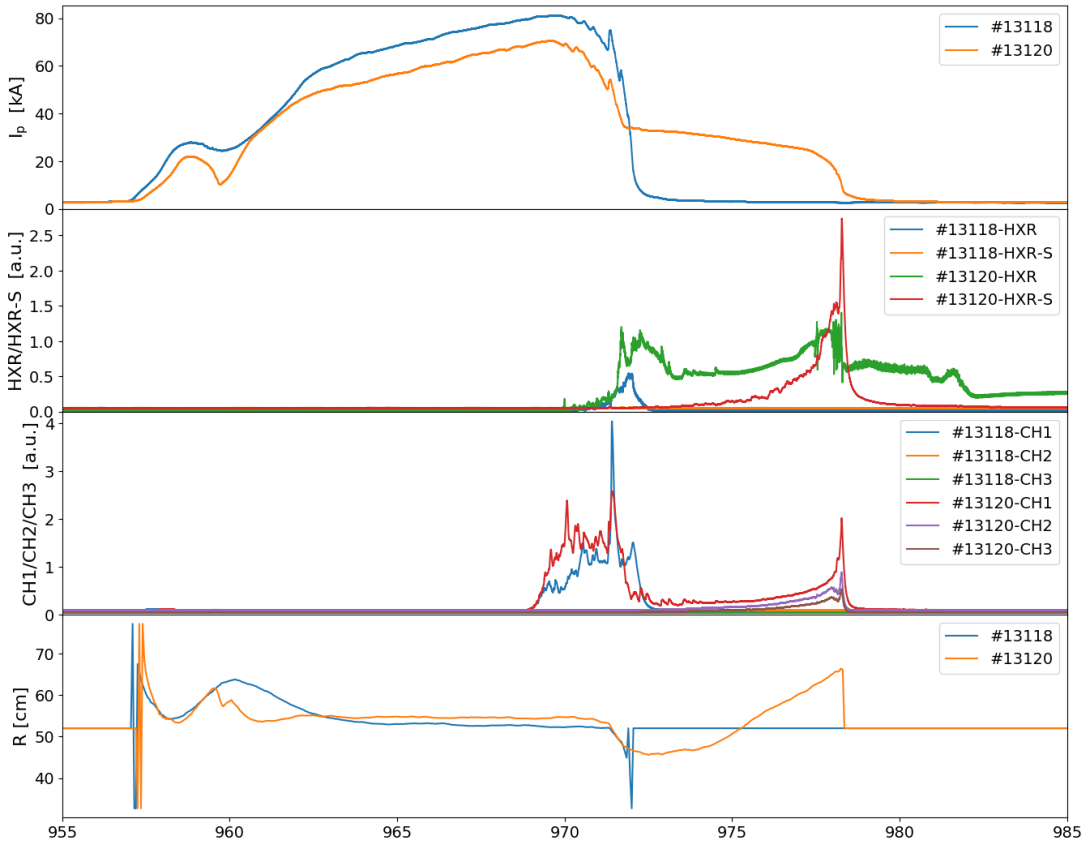

Figure 4.13: Comparison of shots #13118 and #13120.

can clearly seen that in discharge #10921 is not visible strong emission of Cherenkov radiation during disruption, but in #13120 is. As was sad above, this change in evolution of signals can be caused by position of the detector, by installation of rezistor or by detector failure. Due to short support of the detector a reasonable radial position scan could no be done.

Despite the reasons that are mentioned above the significant change in evolution of signals from the Cherenkov detector may be most likely caused by different toroidal position of the protection limiter. During experimental campaign, which was held in the year 2015, the protection limiter was not placed between ports 1 and 16 as is illustrated in Fig. 4.1, but was situated between ports 9 and 10. This toroidal is much closer to the toroidal position of the Cherenkov detector.

4.4.2 RE beam statistics

In this section some statistics focused on the characterization of post-disruptive beams is presented. Firstly, the influence of losses of RE seed, which is created during the ramp-up phase due to high loop voltage and is lost during disruption, is investigated. Furthermore, dependence of the plasma current carried by the RE after the disruption I_{beam} on loses of RE during RE beam phase is studied.

Previous section deals with the basic description of the post-disruptive beams. The rapid termination of the plasma was always marked by strong emission of the Cherenkov radiation. Burst of the Cherenkov radiation during the disruption correspond to losses of RE seed, which is responsible for creation of the RE beam. One of important questions is, how losses during the disruption influence creation of RE beam. Because the signal from the Cherenkov detector is caused by the flux of electron through the

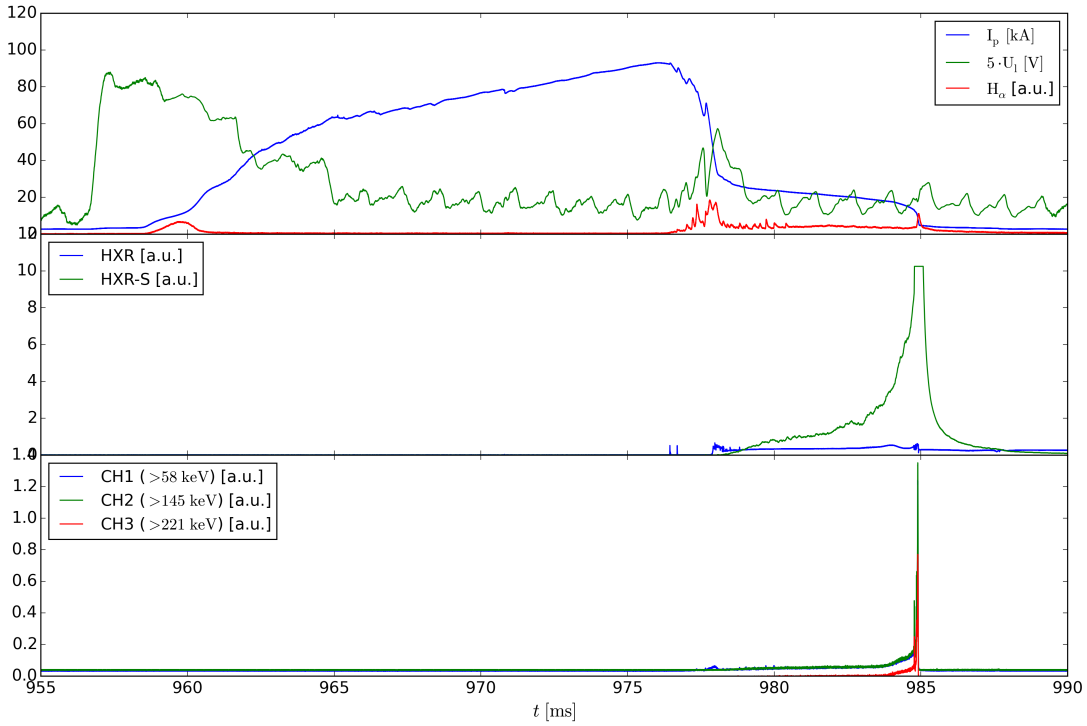

Figure 4.14: Evolution of the basic plasma parameters during induced Argon disruption with creation of RE beam (#10921).

detector, this signal can be interpreted as amount of particles, which are lost from the plasma. In Fig. 4.15 dependence of current carried by RE after disruption on electron fluency detected during by the first channel (> 58 keV) of the Cherenkov detector during the disruption is displayed. As can be seen from this figure, for high values of electron fluency the RE beam is no created, but figure shows no clear trend. The same situation is repeated in Fig. 4.16, 4.17 and 4.18, where dependence of I_{beam} on total flux of HXR radiation recorded by scintillation detectors denoted as HXR and HXR2 and total flux of neutrons are shown. Each figure suggests, that may exist some threshold for RE beam creation. As it was already mentioned in the previous section, during the disruption particles in energetic range 58 − 145 keV are predominantly lost. Non-existence of signal from second and third channel of the Cherenkov detector can be explained by the fact, that electrons have been not sufficiently accelerated yet and thus there are no electrons with energy higher than 145 keV, or more energetic electrons have a better confinement. The second explanation is in agreement with present modelling, which shows that energetic particles are well confined during the disruption and provides a seed for creation of RE beam [42].

On the other hand, in Fig. 4.19, 4.20 and 4.21 dependencies of I_{beam} on average electron fluency detected by all three channels of the Cherenkov detector during the RE beam phase are shown. In this case average electron fluency, which is recorded during RE beam phase, is proportional to average flux of runaway electrons escaping from RE beam. From mentioned figures it can be seen, that losses of runaway electrons increase with current carried by RE after disruption. The stronger RE beam is, the more losses it suffers. This trend is common to all channels of the Cherenkov detector. This suggests, that RE beam is created especially by high energy electrons as can be expected. For the explanation of this effect the more detailed investigation is needed.

Because the HXR radiation is induced by impact of the runaway electrons to the material and thus is cause by the particles escaping from the plasma. We can created similar figures as previous and study the

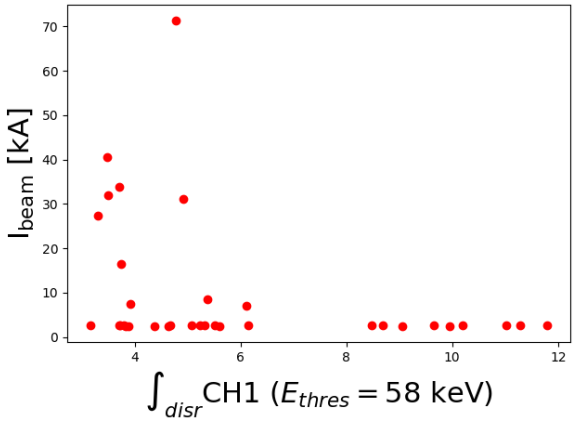

Figure 4.15: Dependence of the current carried by RE after disruption I_{beam} on electron fluency $\int_{disr}$ CH1 detected by the first channel of the Cherenkov detector during the disruption.

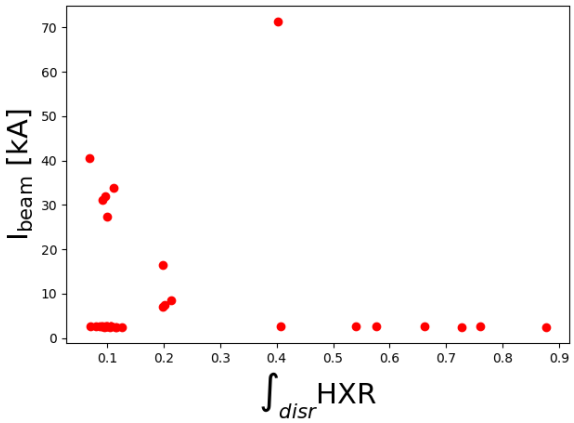

Figure 4.16: Dependence of the current carried by RE after disruption I_{beam} on amount of HXR radiation $\int_{disr}$ HXR detected by scintillation detector denoted as HXR.

dependence of the current carried by RE after disruption I_{beam} on average flux of radiation. In Fig. 4.22 and 4.23 dependence of I_{beam} on the average flux of HXR radiation recorded by scintillation detector denoted as HXR and HXR2 is displayed. It can be clearly seen, that average HXR flux increases with I_{beam} in agreement with results achieved by the Cherenkov detector. Dependence of I_{beam} on average neutron flux is shown in Fig. 4.24. This figure shows the same trend as previous.

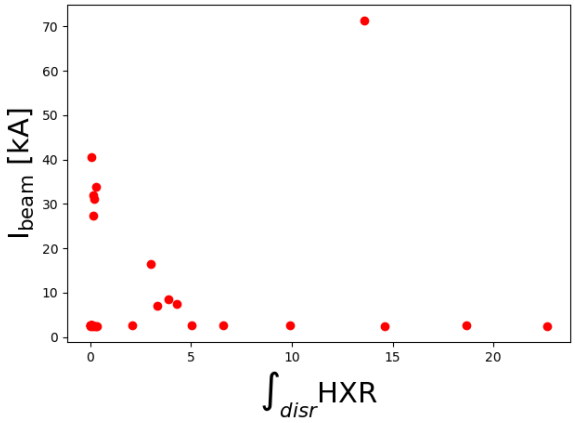

Figure 4.17: Dependence of the current carried by RE after disruption I_{beam} on amount of HXR radiation $\int_{disr}$ HXR detected by scintillation detector denoted as HXR2.

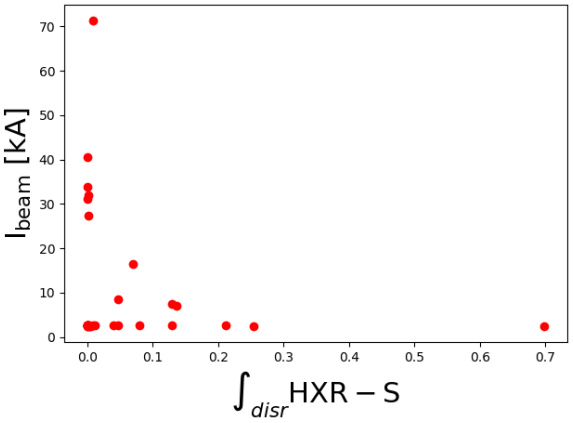

Figure 4.18: Dependence of the current carried by RE after disruption I_{beam} on amount of neutrons $\int_{disr}$ HXR − S detected by scintillation detector denoted as HXR.

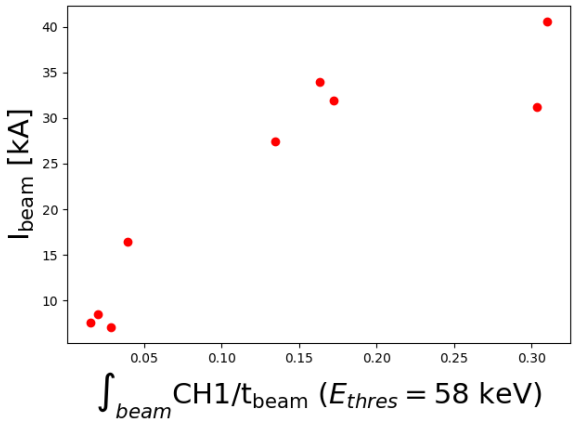

Figure 4.19: Dependence of the current carried by RE after disruption I_{beam} on average electron fluency $\int_{disr}$ CH1/t_{beam} detected by the first channel of the Cherenkov detector during the RE beam phase.

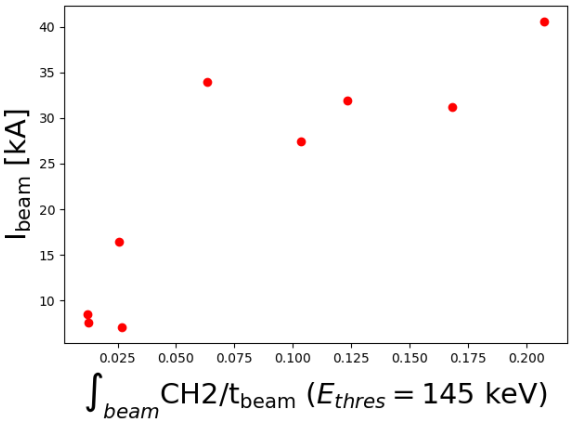

Figure 4.20: Dependence of the current carried by RE after disruption I_{beam} on average electron fluency $\int_{disr}$ CH2/t_{beam} detected by the second channel of the Cherenkov detector during the RE beam phase.

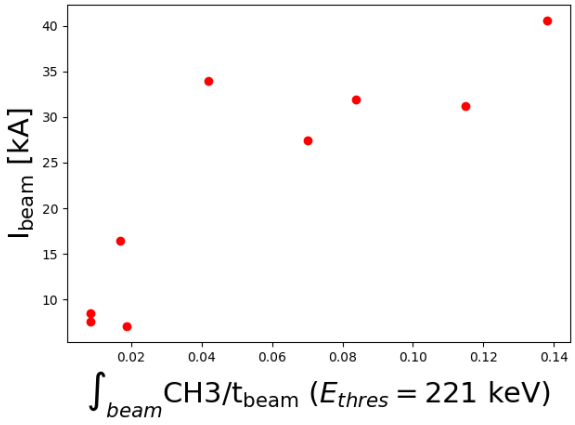

Figure 4.21: Dependence of the current carried by RE after disruption I_{beam} on average electron fluency $\int_{disr} \mathrm{CH3}/t_{beam}$ detected by the third channel of the Cherenkov detector during the RE beam phase.

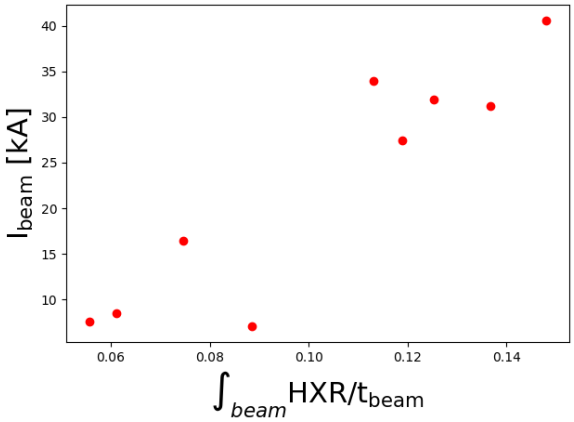

Figure 4.22: Dependence of the current carried by RE after disruption I_{beam} on average flux of HXR radiation $\int_{disr} \mathrm{HXR}/t_{beam}$ detected by scintillation detector denoted as HXR.

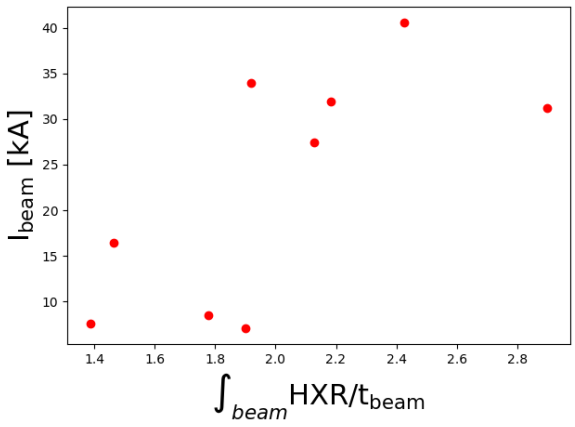

Figure 4.23: Dependence of the current carried by RE after disruption I_{beam} on average flux of HXR radiation $\int_{disr} \mathrm{HXR}/t_{beam}$ detected by scintillation detector denoted as HXR2.

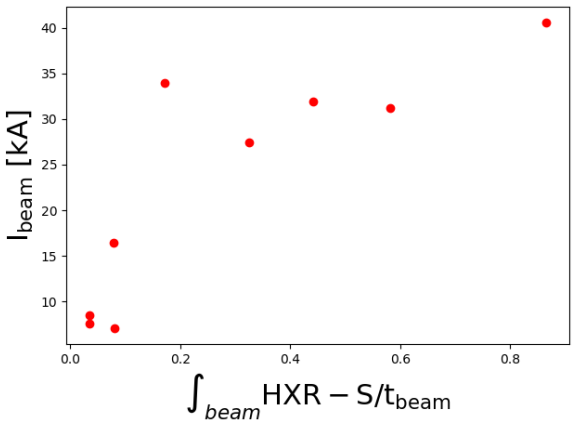

Figure 4.24: Dependence of the current carried by RE after disruption I_{beam} on average flux of neutrons $\int_{disr} \mathrm{HXR-S}/t_{beam}$ detected by scintillation detector denoted as HXR-S.

Conclusion

This work is focused on investigation of the runaway electrons via the Cherenkov detector. Phenomena of the runaway electron is an important part of plasma physics and the understanding to this field of research is crucial for ITER to achieved its mission. Before start of ITER mechanism of generation and losses of runaway electrons and mainly possibilities of their suppression have to be understood.

The first chapter very briefly deals with the runaway electron physics. The generation mechanisms and restriction on maximal attainable energy are given. The second chapter is focused on description of physics behind the Cherenkov radiation. Simple derivation of the properties fo the Cherenkov radiation is shown and the Cherenkov effect is explained. In the third chapter, the Cherenkov detector is described. The second part of this chapter also presents some results from former experiments conducted on different tokamaks (CASTOR, ISSTOK, Tore Supra, FTU) using the Cherenkov detector. The last fourth chapter is focused on experiments, which were carried out on tokamak COMPASS. First of all experimental setup is briefly described and this chapter deals with analysing of experimental data and its interpretation.

First part of the last fourth chapter is focused on description of relationship between signals from the Cherenkov detector and other signals, which indicate losses of runaway electrons. The fact, that even small changes in evolution of basic plasma parameters may influence RE population, is also mentioned. Next part of this chapter is dedicated to the Cherenkov detector radial position scan. Because of capabilities of the Cherenkov detector manipulator this scan has to be carried out on shot-to-shot basis. It requires very good repeatability of discharges including their RE population. With the decreasing radial position, i. g. going towards to the plasma from magnetic low field side, the electron fluency rises and differences between the signals of different channels are increasing. Simple deconvolution of signals from the three-channel Cherenkov detector suggests, that signal in outer radial position is dominantly caused by electrons with energies higher than 221 keV. The fourth section of this chapter is about post-disruptive runaway electron beams, which are triggered by argon induced rapid plasma termination. Firstly, description of this event is given. Secondly, section aims to identify reasons of creation of RE beams and link between losses of RE during plateau phase and plasma current, which is carried by runaway electrons after induced disruption. Influence of position of the Cherenkov detector respect to the protection limiter is also described.

The Cherenkov detector is new promising diagnostic tool, which can provide useful information about dynamics of runaway electrons.

Bibliography

[1] Chen, Francis F.: *Introduction to plasma physics*. Springer Science & Business Media, 2012.

[2] Jaspers, R. J. E.: *Relativistic runaway electrons in tokamak plasmas*. Technische Universiteit Eindhoven, 1995.

[3] Kulhánek, P.: *Úvod do teorie plazmatu*. AGA, Praha, 2013

[4] Dreicer, H.: *Electron and ion runaway in a fully ionized gas. I.*. Physical Review 115.2 (1959): 238.

[5] Dreicer, H.: *Electron and ion runaway in a fully ionized gas. II.*. Physical review 117.2 (1960): 329.

[6] Gurevich, A. V.: *On the theory of runaway electrons*. Sov. Phys. JETP 12.5 (1961): 904-912.

[7] Kruskal, M. D., and Bernstein, I. B.: *Princeton Plasma Physics Lab. Report No. MATT-Q-20*, 1962.

[8] Connor, J. W.; Hastie, R. J.: *Relativistic limitations on runaway electrons*. Nuclear fusion 15.3 (1975): 415.

[9] Smith, Hakan M.; Verwichte E.: *Hot tail runaway electron generation in tokamak disruptions*. Physics of plasmas 15.7 (2008): 072502.

[10] Rosenbluth, M. N.; Putvinski. S. V.: *Theory for avalanche of runaway electrons in tokamaks*. Nuclear Fusion 37.10 (1997): 1355.

[11] Putvinski, S., et al.: *Halo current, runaway electrons and disruption mitigation in ITER*. Plasma Physics and Controlled Fusion 39.12B (1997): B157.

[12] Zehrfeld, H. P.; Fußmann G.; Green, B. J.: *Electric field effects on relativistic charged particle motion in Tokamaks*. Plasma Physics 23.5 (1981): 473.

[13] Knoepfel, H.; Spong, D. A.: *Runaway electrons in toroidal discharges*. Nuclear Fusion 19.6 (1979): 785.

[14] Kvasnica, J.: *Teorie elektromagnetického pole*. 1. vydání: Praha, Academia, 1985

[15] Russo, A. J.: *Effect of ripple on runaway electrons in tokamaks*. Nuclear Fusion 31.1 (1991): 117.

[16] Laurent, L.; Rax, J. M.: *Runaway-ripple interaction in tokamaks*. EUR-CEAFC-1374, 1989.

[17] Čeřovský, J.: *Ubíhající elektrony v tokamacích*. Bakalářská práce (Bachelor project). FNSPE CTU in Prague 2016. `https://physics.fjfi.cvut.cz/publications/FTTF/BP_Jaroslav_Cerovsky.pdf` [29.7.2017]

[18] Ficker, O.: *Generation, looses and detection of runaway electrons in tokamaks*. Master thesis. FNSPE CTU in Prague 2015. https://physics.fjfi.cvut.cz/publications/FTTF/DP_Ondrej_Ficker.pdf [29.7.2017]

[19] Parail, V. V.; Pogutse. O. P.: *The kinetic theory of runaway electron beam instability in a tokamak*. Nuclear Fusion 18.3 (1978): 303.

[20] Cherenkov, P. A.: *Visible emission of clean liquids by action of γ radiation*. Doklady Akademii Nauk SSSR 2 (1934): 451.

[21] Cherenkov, P. A: *Visible radiation produced by electrons moving in a medium with velocities exceeding that of light*. Physical Review 52.4 (1937): 378.

[22] Cogan, P.: *Nanosecond sampling of atmospheric Cherenkov radiation applied to TeV gamma-ray observations of blazars with VERITAS*. Diss. University College Dublin, 2006.

[23] Liu, Chang: *Runaway electrons in tokamaks*. Diss. Priceton University. 2017

[24] Tamm, Ig.: *Radiation emitted by uniformly moving electrons*. Selected Papers. Springer Berlin Heidelberg, 1991. 37-53.

[25] De La Calle Perez, I.: *Detection of High Energy Gamma-rays from X-ray Selected Blazars*. PhD. Thesis. University of Leads. 2003

[26] Plyusnin, V. V.; et al.: *Development of a diagnostic technique based on Cherenkov effect for measurements of fast electrons in fusion devices*. Review of Scientific Instruments 83.8 (2012): 083505.

[27] Jakubowski, L.; Sadowski, M.; Zebrowski J.: *Investigation of new Cerenkov-type detectors for studies of fast electron beams emitted from hot plasma*. Journal of technical physics 38.1 (1997): 141-150.

[28] Jakubowski, L.; Sadowski M.; Zebrowski J.: *Measurements of charged particle beams from plasma focus discharges*. Nuclear fusion 41.6 (2001): 755.

[29] Sadowski, M. J.; Jakubowski L.; Szydlowski A.: *Adaptation of selected diagnostic techniques to magnetic confinement fusion experiments*. Czechoslovak Journal of Physics 54 (2004): C74-C81.

[30] Jakubowski, L.; et al.: *Design and tests of Cherenkov detector for measurements of fast electrons within CASTOR tokamak*. Czechoslovak Journal of Physics 56 (2006): B98-B103.

[31] Jakubowski, L.; et al.: *Design and tests of Cherenkov detector for measurements of fast electrons within CASTOR tokamak*. Czechoslovak Journal of Physics 56 (2006): B98-B103.

[32] Jakubowski, L.; et al.: *Cherenkov Detector For Measurements Of Fast Electrons In CASTOR-Tokamak*. AIP Conference Proceedings. Vol. 996. No. 1. AIP, 2008.

[33] Plyusnin, V. V.; et al.: *Use of Cherenkov-type detectors for measurements of runaway electrons in the ISTTOK tokamak*. Review of Scientific Instruments 79.10 (2008): 10F505.

[34] Jakubowski, L.; et al.: *Measurement of high-energy electrons by means of a Cherenkov detector in ISTTOK tokamak*. Radiation Measurements 45.9 (2010): 1014-1019.

[35] Plyusnin, V. V.; et al.: *Characteristics of four-channel Cherenkov-type detector for measurements of runaway electrons in the ISTTOK tokamak*. Review of Scientific Instruments 81.10 (2010): 10D304.

[36] Jakubowski, L.; et al.: *Correlation of Electron Beams and Hard X-ray Emissions in ISTTOK Tokamak*. Contributions to Plasma Physics 53.9 (2013): 615-622.

[37] Jakubowski, L.; et al.: *Cherenkov-type diamond detectors for measurements of fast electrons in the TORE-SUPRA tokamak*. Review of Scientific Instruments 81.1 (2010): 013504.

[38] Jakubowski, L.; et al: *Note: Measurements of fast electrons in the TORE-SUPRA tokamak by means of modified Cherenkov-type diamond detector*. Review of Scientific Instruments 84.1 (2013): 016107.

[39] Causa, F.; et al: *Cherenkov emission provides detailed picture of non-thermal electron dynamics in the presence of magnetic islands*. Nuclear Fusion 55.12 (2015): 123021.

[40] SAINT-LAURENT, F.: *Disruption and runaways electron mitigation studies on Tore Supra* EXS 2: 16, 2010.

[41] Ficker, O.; et al.: *Losses of runaway electrons in MHD-active plasmas of the COMPASS tokamak*. Nuclear Fusion 57.7, 2017.

[42] Sommariva, C.; et al.: *Modeling runaway electron dynamics in realistic fields from 3D non-linear MHD disruption simulations*. 43rd EPS Conf. on Plasma Physics. 2016.